

# **Load Flow Feasibility under Extreme Contingencies**

Iman Khosravi-Dehkordi

B.Eng. (McGill University, Montreal, Canada)

A thesis submitted to the department of Electrical Engineering in partial fulfillment of the  
requirements for the degree of  
Masters of Engineering

Department of Electrical Engineering,

McGill University,

Montreal, Quebec, Canada

(c) December, 2007



Library and  
Archives Canada

Published Heritage  
Branch

395 Wellington Street  
Ottawa ON K1A 0N4  
Canada

Bibliothèque et  
Archives Canada

Direction du  
Patrimoine de l'édition

395, rue Wellington  
Ottawa ON K1A 0N4  
Canada

*Your file* *Votre référence*  
*ISBN: 978-0-494-51463-4*  
*Our file* *Notre référence*  
*ISBN: 978-0-494-51463-4*

**NOTICE:**

The author has granted a non-exclusive license allowing Library and Archives Canada to reproduce, publish, archive, preserve, conserve, communicate to the public by telecommunication or on the Internet, loan, distribute and sell theses worldwide, for commercial or non-commercial purposes, in microform, paper, electronic and/or any other formats.

The author retains copyright ownership and moral rights in this thesis. Neither the thesis nor substantial extracts from it may be printed or otherwise reproduced without the author's permission.

**AVIS:**

L'auteur a accordé une licence non exclusive permettant à la Bibliothèque et Archives Canada de reproduire, publier, archiver, sauvegarder, conserver, transmettre au public par télécommunication ou par l'Internet, prêter, distribuer et vendre des thèses partout dans le monde, à des fins commerciales ou autres, sur support microforme, papier, électronique et/ou autres formats.

L'auteur conserve la propriété du droit d'auteur et des droits moraux qui protègent cette thèse. Ni la thèse ni des extraits substantiels de celle-ci ne doivent être imprimés ou autrement reproduits sans son autorisation.

---

In compliance with the Canadian Privacy Act some supporting forms may have been removed from this thesis.

While these forms may be included in the document page count, their removal does not represent any loss of content from the thesis.

Conformément à la loi canadienne sur la protection de la vie privée, quelques formulaires secondaires ont été enlevés de cette thèse.

Bien que ces formulaires aient inclus dans la pagination, il n'y aura aucun contenu manquant.

  
**Canada**

## Abstract

This thesis examines the problem of load flow feasibility, in other words, the conditions under which a power network characterized by the load flow equations has a steady-state solution. In this thesis, we are particularly interested in load flow feasibility in the presence of extreme contingencies such as the outage of several transmission lines.

Denoting the load flow equations by  $\underline{z} = \underline{f}(\underline{x})$  where  $\underline{z}$  is the vector of specified injections (the real and reactive bus demands, the specified real power bus generations and the specified bus voltage levels), the question addressed is whether there exists a real solution  $\underline{x}$  to  $\underline{z} = \underline{f}(\underline{x})$  where  $\underline{x}$  is the vector of unknown bus voltage magnitudes at load buses and unknown bus voltage phase angles at all buses but the reference bus. Attacking this problem via conventional load flow algorithms has a major drawback, principally the fact that such algorithms do not converge when the load flow injections  $\underline{z}$  define or are close to defining an infeasible load flow. In such cases, lack of convergence may be due to load flow infeasibility or simply to the ill-conditioning of the load flow Jacobian matrix.

This thesis therefore makes use of the method of supporting hyperplanes to characterize the load flow feasibility region, defined as the set the injections  $\underline{z}$  for which there exists a real solution  $\underline{x}$  to the load flow equations. Supporting hyperplanes allow us to calculate the so-called load flow feasibility margin, which determines whether a given injection is feasible or not as well as measuring how close the injection is to the feasibility boundary. This requires solving a generalized eigenvalue problem and a corresponding optimization for the closest feasible boundary point to the given injection.

The effect of extreme network contingencies on the feasibility of a given injection is examined for two main cases: those contingencies that affect the feasibility region such as line outages and those that change the given injection itself such as an increase in VAR demand or the loss of a generator. The results show that the hyperplane method is a

powerful tool for analyzing the effect of extreme contingencies on the feasibility of a power network.

## Résumé

Ce mémoire étudie le problème de la faisabilité de l'écoulement d'énergie, c'est-à-dire aux conditions sous lesquelles un réseau électrique, caractérisé par les équations d'écoulement d'énergie, a une solution stationnaire. Il analyse plus spécifiquement la faisabilité de l'écoulement d'énergie en cas d'accident, comme par exemple la panne de plusieurs lignes électriques.

On note  $\underline{z} = \underline{f}(\underline{x})$  l'équation vectorielle de l'écoulement d'énergie, où  $\underline{z}$  est l'injection d'énergie (la demande en puissance réelle et réactive, la production de puissance réelle et la tension à chaque bus). Existe-t-il alors une solution  $\underline{x}$  réelle? Le vecteur  $\underline{x}$  représente les modules et les phases des tensions aux bus de charge. L'ensemble de ces valeurs sont inconnues, à l'exception de la phase au bus de référence qui est nulle. Les algorithmes traditionnels présentent un défaut majeur: ils ne convergent pas lorsque l'injection d'énergie  $\underline{z}$  définit un flux d'énergie irréalisable ou proche de l'être. Ceci peut être causé par un écoulement d'énergie irréalisable ou simplement par une matrice Jacobienne de l'écoulement d'énergie mal conditionnée.

Cette étude utilise la méthode de séparation des convexes pour définir les limites de faisabilité de l'écoulement d'énergie, c'est-à-dire les injections  $\underline{z}$  pour lesquelles il existe une solution  $\underline{x}$  réelle. La séparation des convexes permet de calculer la marge de faisabilité de l'écoulement, qui détermine si une injection est réalisable mais qui aussi mesure sa distance aux limites de faisabilité. Cette méthode nécessite la résolution d'un problème aux valeurs propres généralisé, et du problème d'optimisation correspondant afin trouver la limite de faisabilité la plus proche de l'injection.

Les conséquences d'un événement exceptionnel sur la faisabilité d'une injection donnée sont analysées dans deux cas: d'une part les événements qui affectent les limites de faisabilité, comme par exemple l'arrêt de fonctionnement de lignes électriques, et d'autre part ceux qui modifient l'injection d'énergie, par exemple une augmentation de la

demande en VAR (volt ampère réactif) ou la panne d'un générateur. Les résultats montrent que la méthode de séparation des convexes est un outil puissant pour déterminer les conséquences d'un événement extrême sur la faisabilité d'un réseau électrique

## Acknowledgments

I would like to gratefully thank my supervisor Professor Frank D. Galiana for his support, guidance, thorough discussion and supervision during my entire graduate studies. I would like to extend my gratitude to Dr. Hadi Banakar for his insightful suggestions and expertise through this work. My warm and sincere thank goes to the graduate students in the power research group, especially, Mr. Jose Restrepo, Mr. Changling Luo, Mr. Saadat Qadri and Mr. Hassan Ebrahim A.Rahman for their support, kindness and help to allow the completion of this thesis.

# Table of Contents

Table of Contents .....	vi
List of Tables .....	viii
List of Figures .....	ix
List of Symbols .....	xi
Chapter 1: Introduction .....	1
1.1 General .....	1
1.2 Load flow feasibility example .....	2
1.3 Motivation and methodology for the investigation of load flow feasibility .....	5
1.4 Goal of the thesis .....	7
1.5 Outline of the thesis .....	8
Chapter 2: Characterizing Load Flow Feasibility .....	8
Chapter 3: Study Cases of Load Flow Feasibility .....	9
Chapter 4: Conclusion .....	9
Chapter 2: Characterizing Load Flow Feasibility .....	10
2.1 Load flow .....	10
2.1.1 Polar and Rectangular Coordinate Forms .....	10
2.1.2 Hand solved example .....	12
2.2 Feasibility Region .....	15
2.2.1 Feasibility Region $R_z$ .....	15
2.2.2 Feasibility Region on a Plane .....	17
2.2.3 Hand solved example to illustrate notion of feasibility region on a plane .....	19
2.3 Supporting Hyperplanes .....	23
2.3.1 Definition and Solution Method .....	23
2.3.2 J-Matrix Implementation .....	26
2.3.3 Hand solved example of the J-matrix and supporting hyperplanes .....	28
2.4 Closest Boundary Injection .....	33
2.4.1 Feasibility Margin .....	33
2.4.2 Optimization Scheme .....	36
Chapter 3 : Study Cases of Load Flow Infeasibility .....	42
3.1 Feasibility boundary movement .....	43
3.1.1 Bus type change .....	43
3.1.2 Change in network structure .....	46
3.2 Movement of the nodal injection vector .....	53
3.2.1 Gradual change .....	53
3.2.2 Sudden change .....	61



Chapter 4: Conclusions .....	67
4.1 Summary .....	67
4.2 Suggestions for Further Research .....	68
Bibliography .....	69
Appendix A .....	71
The Gradient.....	71
Appendix B.....	74

## List of Tables

<b>Table 3-1:</b> Load flow for 5-bus network #1 .....	45
<b>Table 3-2:</b> Feasibility margins for a change in bus type .....	45
<b>Table 3-3:</b> Bus injections for 14-bus network .....	47
<b>Table 3-4:</b> Line removal results.....	48
<b>Table 3-5:</b> Line removal results with line 13 already out .....	49
<b>Table 3-6:</b> Line removal results with lines 13 and 7 already out .....	50
<b>Table 3-7:</b> New bus injections.....	51
<b>Table 3-8:</b> Line removal results.....	52
<b>Table 3-9:</b> Load flow.....	54
<b>Table 3-10:</b> Change in feasibility margin due to the change in $Q$ .....	54
<b>Table 3-11:</b> Load flow for 5-bus network #2 .....	59
<b>Table 3-12:</b> $\alpha$ values for the given injection $\underline{z}_g$ .....	60
<b>Table 3-13:</b> Feasibility margin due to imaginary power decrease at bus 1 and 3 .....	60
<b>Table 3-14:</b> Original load flow for 5-bus network #1.....	62
<b>Table 3-15:</b> Load flow for 5-bus network #1 after loss of the generator at bus 4 .....	63
<b>Table 3-16:</b> Load flow for 5-bus network #1 after loss of the generator at bus 5 .....	63
<b>Table 3-17:</b> Change in feasibility margin for the loss of each generator .....	63
<b>Table 3-18:</b> Original load flow for 5-bus network #1 (Higher Load).....	64
<b>Table 3-19:</b> Load flow for 5-bus network #1 (Higher Load) after loss of the generator at bus 4.....	65
<b>Table 3-20:</b> Load flow for 5-bus network #1 (Higher Load) after loss of the generator at bus 5.....	65
<b>Table 3-21:</b> Change in feasibility margin for the loss of each generator .....	65
<b>Table B-1:</b> Line data of 5-bus example #1 .....	74
<b>Table B-2:</b> Line data of 5-bus example #2.....	74
<b>Table B-3:</b> Line data of 14-bus example.....	75

## List of Figures

<b>Figure 1-1:</b> 2-bus network example .....	2
<b>Figure 1-2:</b> Feasibility region for the 2-bus network.....	3
<b>Figure 1-3:</b> Closest boundary injection .....	4
<b>Figure 1-4:</b> Plot of the voltage at bus 2 versus $Q_2$ .....	5
<b>Figure 1-5:</b> Supporting hyperplanes.....	6
<b>Figure 1-6:</b> Effect of line outage on the feasibility boundary.....	7
<b>Figure 2-1:</b> 2-bus network example with one $PQ$ bus.....	13
<b>Figure 2-2:</b> Feasibility region $R_z$ of a 3-dimensional injection space .....	16
<b>Figure 2-3:</b> Feasibility region lies above a set of hyperplanes .....	17
<b>Figure 2-4 (a):</b> Geometrical illustration of feasibility region on a plane $P_{z_0}$ (the plane $\underline{z}_0^T \underline{z} = k$ does not intersect all rays in $R_z$ ) .....	18
<b>Figure 2-4 (b):</b> Geometrical illustration of feasibility region on a plane $P_{z_0}$ (the plane $\underline{z}_0^T \underline{z} = k$ intersects all rays in $R_z$ ) .....	18
<b>Figure 2-5:</b> Load flow feasibility region $R_z$ of the network in Figure 2-1 .....	20
<b>Figure 2-6:</b> Feasibility region on a plane $P_{z_0}$ (the plane $\underline{z}_0^T \underline{z} = k$ does not intersect all rays in $R_z$ ) ....	21
<b>Figure 2-7:</b> Feasibility region on a plane $P_{z_0}$ (the plane $\underline{z}_0^T \underline{z} = k$ intersects all rays in $R_z$ ) .....	22
<b>Figure 2-8 (a):</b> Example of supporting hyperplanes $\underline{\alpha}^T \underline{z} = 0$ of the load flow feasibility region $R_z$ ....	23
<b>Figure 2-8 (b):</b> 2-dimensional feasibility surface $P_{z_0}$ .....	24
<b>Figure 2-9 (a):</b> Intersection of the plane $\underline{z}_1^T \underline{z} = c$ with $P_{z_0}$ for various values of $c$ .....	24
<b>Figure 2-9 (b):</b> Intersection of the plane $\underline{z}_1^T \underline{z} = c$ with $P_{z_0}$ for various values of $c$ .....	25
<b>Figure 2-10:</b> 2-Bus network example with one $PQ$ bus .....	28
<b>Figure 2-11:</b> Geometrical illustration of the feasibility margin FM of a given injection $\underline{z}_g$ .....	34
<b>Figure 2-12:</b> Flowchart of the program computing feasibility margin .....	38
<b>Figure 2-13 (a):</b> Illustration of the search process for the closest boundary injection $\underline{z}_b^*$ .....	39
<b>Figure 2-13 (b):</b> 2-dimensional feasibility surface $P_{z_0}$ .....	40
<b>Figure 2-14:</b> Flowchart of the optimization program .....	40
<b>Figure 3-1:</b> Feasibility boundary movement .....	42
<b>Figure 3-2:</b> Injection vector movement .....	43
<b>Figure 3-3:</b> 5-Bus network #1 .....	44
<b>Figure 3-4:</b> 14-bus Network.....	46
<b>Figure 3-5:</b> Feasibility margin for different line removals.....	48
<b>Figure 3-6:</b> Feasibility margin for different line removals with line 13 already out .....	49

<b>Figure 3-7:</b> Feasibility margin for different line removals with lines 13 and 7 already out .....	50
<b>Figure 3-8:</b> Feasibility margin for different line removals.....	52
<b>Figure 3-9:</b> 3-bus network .....	53
<b>Figure 3-10:</b> Graph of the change in feasibility margin as $Q_2$ decreases.....	55
<b>Figure 3-11:</b> Change in the magnitude of the nodal voltages.....	56
<b>Figure 3-12:</b> Change in the angle difference for each line.....	57
<b>Figure 3-13:</b> Change in the total transmission loss in the network .....	57
<b>Figure 3-14:</b> Change in the eigenvalues of the Jacobian .....	58
<b>Figure 3-15:</b> 5-Bus network #2 .....	59
<b>Figure 3-16:</b> Feasibility margin due to imaginary power decrease at bus 1 and 3 .....	61
<b>Figure 3-17:</b> 5-bus network #1 .....	62

## List of Symbols

$N$	Number of buses in the network, including the slack bus.
$npq$	Number of PQ buses.
$\bar{S}_i$	Net complex power injected into bus $i$ .
$P_i$	Net real power injected into bus $i$ .
$Q_i$	Net reactive power injected into bus $i$ .
$\bar{V}_i$	Complex voltage at bus $i$ .
$\bar{I}_i$	Complex current at bus $i$ .
$V_i$	Voltage magnitude at bus $i$ .
$\delta_i$	Phase angle of $\bar{V}_i$ .
$e_i$	Real part of $\bar{V}_i$ .
$f_i$	Imaginary part of $\bar{V}_i$ .
$\underline{e}$	$(e_1, e_2, \dots, e_N)^T$ .
$\underline{f}$	$(f_1, f_2, \dots, f_N)^T$ .
$\underline{x}$	$(\underline{e}, \underline{f})$ .
$\bar{Y}$	Complex bus admittance matrix.
$\underline{G}$	Real part of $\bar{Y}$ .
$\underline{B}$	Imaginary part of $\bar{Y}$ .
$z_i$	Net injection at bus $i$ .
$\underline{z}$	$(z_1, z_2, \dots, z_{2N-1})^T$ .
$\underline{z} = \underline{F}(\underline{x})$	Load flow equations.
$R_z$	Load flow feasibility region $\in R^{2N-1}$ .
$\frac{\partial \underline{z}}{\partial \underline{x}}$	Jacobian of the load flow equations.
$\underline{L}(\underline{x})$	Half of the Jacobian of the load flow equations.

$\underline{J}_i$	Real symmetric matrix.
$\lambda$	Eigenvalue.
$\underline{z}_b$	Injection $\underline{z}$ on the boundary of $R_z$ .
$\underline{\alpha}^T \underline{z} = 0$	Supporting hyperplane of $R_z$ .
$R_\alpha$	Set of supporting hyperplanes
$X_l$	Reactance of a transmission line.
$\underline{z}_0$	Constant vector.
$\underline{z}_0^T \underline{z} = 0$	Plane intersecting $R_z$ .
$P_{z_0}$	Feasibility region on a plane.
$\underline{z}_1$	Search vector.
$\underline{z}_g$	Given injection.
$\underline{\alpha}^*$	Set of supporting hyperplanes
$\underline{z}_b^*$	Closest boundary injection to the given injection $\underline{z}_g$ .
FM	Steady state feasibility margin.
$\theta$	Angle between $\underline{\alpha}$ and $\underline{z}_g$ .
$D(\underline{\alpha}, \underline{z}_g)$	Feasibility measure forming the objective function of FM

## Chapter 1: Introduction

### 1.1 General

Modern power systems today are comprised of hundreds of transmission lines, substations and power plants, and are furthermore interconnected with neighbouring utilities in the interest of reducing cost and achieving higher reliability [1]. Concern for pollution in the environment and health hazards from radiation effects have led to siting the thermal and nuclear plants in locations remote from the load centers [2]. There is also the integration of numerous wind farms in the network. The difficulties in obtaining right-of-way have caused delays in construction of transmission lines and have led to the use of multi-circuit lines. All these factors contribute to making power systems highly complex to design and operate, and vulnerable to disturbances or equipment failures [1].

One of the most important aspects of a power system analysis with theoretical and practical applications in planning and operation is its steady-state behaviour as determined by the load flow equations. These define the relationship between the injected real and reactive power and the complex voltage at the buses of a power network. Load flow feasibility is concerned with fundamental theoretical limitations on the load flow equations due to the nonlinear relationship between power  $\underline{z}$  and voltage  $\underline{x}$ , which in general has the form, [3]

$$\underline{z} = \underline{F}(\underline{x}) \quad (1.1)$$

In Equation (1.1),  $\underline{x}$  is the vector of the real and imaginary parts of the complex bus voltages while  $\underline{z}$  is the bus injection vector, comprised of the specified net real and reactive power demands at the load buses and the net real power generations and voltage magnitudes at the generation buses.

One of the main objectives in load flow feasibility analysis is to characterize the conditions on the load flow injections  $\underline{z}$  for which a real steady-state equilibrium solution,  $\underline{x}$ , exists. Since the set of algebraic equations is nonlinear, there exist bus injection vectors for which no real voltage solution exists. Those injection vectors,  $\underline{z}$ ,

which have a real voltage solution,  $\underline{x}$  are defined to be feasible, otherwise the injection  $\underline{z}$  is infeasible [6].

In the space of all possible injections,  $\underline{z}$ , one can define a region  $R_z$  comprising all feasible injections called the load flow feasibility region.

## 1.2 Load flow feasibility example

To illustrate the notion of a load flow feasibility region, consider the following example.

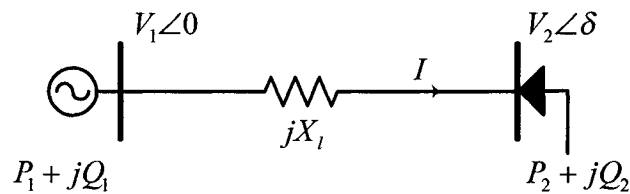


**Figure 1-1:** 2-bus network example

In Figure 1-1, a 2-bus network is shown. The injections at bus 2 include the real and imaginary power values  $P_2$  and  $Q_2$ . The load flow equations which are explained in more detail in section 2.1.2, define  $P_2$  and  $Q_2$  in terms of the nodal voltage components, which in polar form are  $V_1$ ,  $V_2$  and the angle  $\delta$ .

$$\begin{aligned} P_2 &= \frac{V_1 V_2 \sin(\delta)}{X_l} \\ Q_2 &= \frac{V_2^2 - V_1 V_2 \cos(\delta)}{X_l} \end{aligned} \quad (1.2)$$

Equations (1.2) can be rewritten as the following,

$$\begin{aligned} \sin(\delta) &= \frac{X_l P_2}{V_1 V_2} \\ \cos(\delta) &= \frac{V_2^2 + X_l Q_2}{V_1 V_2} \end{aligned} \quad (1.3)$$

The angle  $\delta$  can be eliminated from Equations (1.3) using the identity  $\sin^2(\delta) + \cos^2(\delta) = 1$ , resulting in,



$$(V_2^2)^2 + V_2^2 [V_1^2 + 2X_l Q_2] + X_l^2 [P_2^2 + Q_2^2] = 0 \quad (1.4)$$

For a given  $V_1$ , in order to have load flow feasibility, a real solution must exist for  $V_2^2$ . This means that the determinant of the quadratic Equation (1.4) must be positive or zero.

$$\Delta = [V_1^2 + 2X_l Q_2]^2 - 4X_l^2 [P_2^2 + Q_2^2] \geq 0 \quad (1.5)$$

Rearranging (1.5), we conclude that the specified load flow injections  $P_2$ ,  $Q_2$  and  $V_1^2$  must satisfy the feasibility inequality.

$$V_1^4 + 4V_1^2 (X_l) Q_2 - 4(X_l)^2 P_2^2 \geq 0 \quad (1.6)$$

This can be shown graphically in the space of injections  $P_2$  and  $Q_2$  for a given  $V_1^2$ .

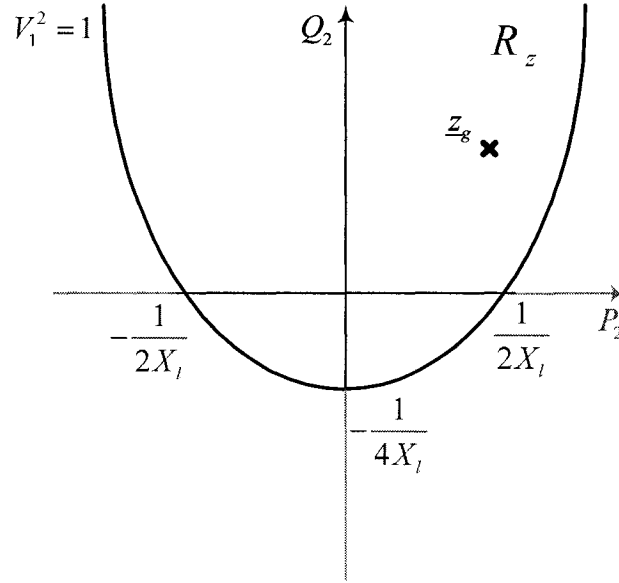


**Figure 1-2:** Feasibility region for the 2-bus network

In Figure 1-2, any given injection  $\underline{z}_g = [P_2, Q_2]$  above the plot defined by inequality (1.6) is feasible.

It is important to identify the presence of an injection close to or outside the boundary  $R_z$ , since proximity to the boundary leads to voltage collapse and being outside the boundary leads to infeasibility [7].

Let us consider the example of Figure 1-2. Starting from a given point with zero real and imaginary power injections, slowly decrease the imaginary power and move towards the feasibility boundary.

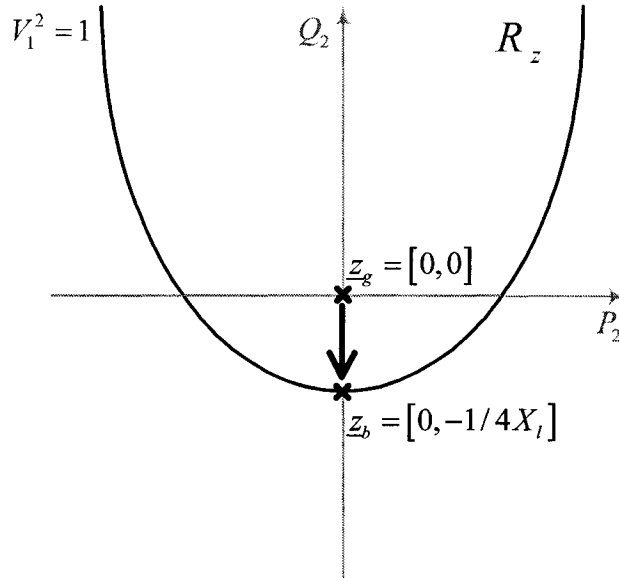


**Figure 1-3:** Closest boundary injection

As seen in Figure 1-3, this trajectory eventually hits injection  $z_b$  on the boundary of the feasibility region with zero real power and  $Q_2 = -1/4X_l$ . An injection with  $Q_2 < -1/4X_l$  will result in a negative determinant in the Equation (1.5) and is infeasible.

In addition, the value of the voltage at bus 2,  $V_2^2$ , drops as the imaginary power is decreased to  $-1/4X_l$ . This collapse of voltage which happens at  $z_b$  on the feasibility boundary and is due to lack of imaginary power support at bus 2 is shown in Figure 1-4.

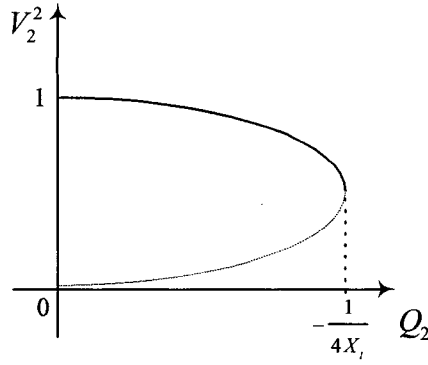


**Figure 1-4:** Plot of the voltage at bus 2 versus  $Q_2$

### 1.3 Motivation and methodology for the investigation of load flow feasibility

Significant effort has been devoted to define the boundaries of the feasibility region [8]. A simple method to do so is to repeatedly solve conventional load flows under increased loading as shown in Figure 1-3. This method however, requires extensive load flow calculations. Moreover, as the injection comes closer to the boundary of feasibility, the Jacobian matrix required to solve the load flow equations becomes more ill-conditioned. This load flow method determines the maximum possible variation of real and reactive power injections before a Jacobian singularity condition is reached [9].

One problem with this approach is that, since the load flow might cease to converge for an injection in the feasible region close to the boundary, one cannot conclude whether an injection is infeasible or the problem is numerical.

In this thesis, an alternative approach is used to analyse the boundary of the feasibility region and, more specifically, to find the closest boundary injection. This approach characterizes the feasibility region with a set of supporting hyperplanes such that  $\underline{\alpha}^T \underline{z} \geq 0$  for  $\underline{z} \in R_z$ , where  $\underline{\alpha}$  is the normal vector of the supporting hyperplane [6].

As shown in this thesis, there exist infinitely many supporting hyperplanes. Of particular interest among the many supporting hyperplanes, we will show how compute the closest one to a given injection vector, as illustrated in Figure 1-5.

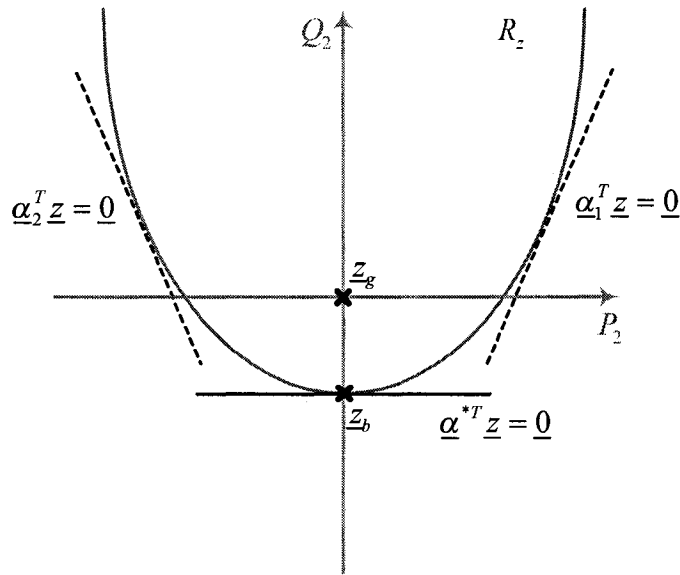


**Figure 1-5:** Supporting hyperplanes

As seen in Figure 1-5, the feasibility boundary is locally approximated by supporting hyperplanes such as  $\underline{\alpha}_1^T \underline{z} = \underline{0}$  and  $\underline{\alpha}_2^T \underline{z} = \underline{0}$ . However the closest supporting hyperplane is  $\underline{\alpha}^{*T} \underline{z} = \underline{0}$ , whose intersection with the feasibility boundary is  $\underline{z}_b$ , the closest boundary injection to  $\underline{z}_g$ .

Furthermore, the hyperplane method defines a feasibility margin (FM) to measure the degree of feasibility of a given injection [6],

$$FM = \cos(\theta) = \frac{\underline{z}_g^T \underline{\alpha}}{\|\underline{z}_g\| \|\underline{\alpha}\|} \quad (1.7)$$

Where  $\theta$  is the angle between the given injection  $\underline{z}_g$  and  $\underline{\alpha}^*$  the normal vector of the closest boundary hyperplane. The FM is positive for feasible injections, becomes zero on the feasibility boundary and is negative for infeasible injections.

Since without load flow feasibility no steady-state equilibrium is possible, the power system becomes unstable. Thus understanding the nature of load flow feasibility is crucial in power system planning and operation, particularly after line outages or major changes

in the injections, not uncommon occurrences [10]. Contingencies affect load flow feasibility in different ways. Thus, line outages change the structure of a network. This results in a change in the feasibility boundary which can affect the feasibility of a given injection as shown in Figure 1-6.

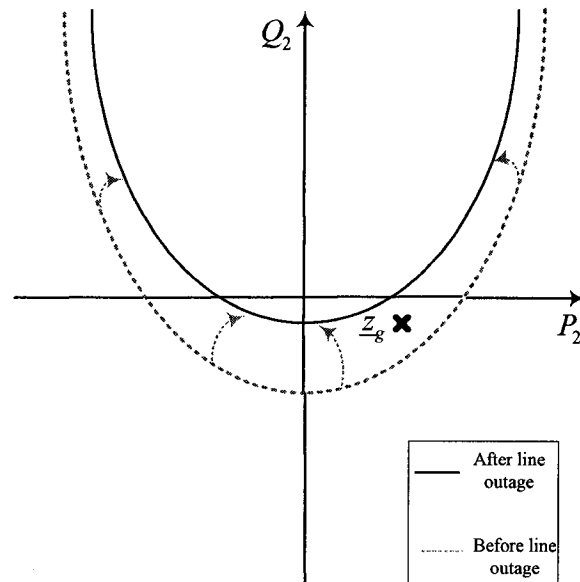


**Figure 1-6:** Effect of line outage on the feasibility boundary

It can be seen that a line outage results in a decrease in the size of  $R_z$ , which leads to infeasibility for the shown injection  $z_g$ .

Another kind of contingency can result in movement of the given injection itself. This was shown previously in the example of Figure 1-3., where the decrease in  $Q_2$ , which can occur when a capacitor bank or SVC goes offline, drives the system towards infeasibility. Chapter 3 discusses these examples in more detail.

#### 1.4 Goal of the thesis

This thesis examines in detail the method of supporting hyperplanes to study power grid load flow feasibility. This method proves to be much more powerful than conventional load flow in finding points on the boundary of the feasibility region,  $R_z$ , and specially the

closest injection on the boundary of feasibility to a given injection,  $\underline{z}_g$ , which is used to measure the degree of the feasibility of that injection.

Specifically, this thesis examines the impact of extreme contingencies on power system feasibility. Two classes of extreme contingencies are defined here. The first class is made up of those events that modify the given injection,  $\underline{z}_g$ , such that it is driven towards infeasibility. The second class of events are those that result in change to the power network causing the feasibility region,  $R_z$ , to change.

Furthermore, a contingency is categorized as gradual and sudden. Events such as an increase in VAR demand result in a gradual movement of the injection towards infeasibility, whereas sudden loss of lines or generators could make an injection infeasible immediately. Moreover, the impact of a contingency can vary with system demand level.

## **1.5 Outline of the thesis**

### **Chapter 2: Characterizing Load Flow Feasibility**

This chapter describes the supporting hyperplane method. It first introduces load flow in polar and rectangular coordinates, accompanied by an example. Then, the notions of feasibility plane and region are defined. The example is used to provide insight into these notions.

Next, supporting hyperplanes, the eigenvalue problem and the notion of the closest boundary injection are explained in detail using the example.

Finally the steps taken to implement the supporting hyperplane method in MATLAB are described.

### **Chapter 3: Study Cases of Load Flow Feasibility**

In this chapter, different types of contingencies and their analysis through in the hyperplane method are presented. Certain examples study changes in the feasibility region due to transmission line outage. Others look at changes in the given injection due to loss of VAR support or generation, which may also lead to a corresponding bus type change.

The effect of the loading of the power network on the severity of a contingency from the load flow feasibility point of view is also examined.

### **Chapter 4: Conclusion**

This is the conclusion chapter. It includes a summary of the work presented in the thesis as well as recommendations for future work.

## Chapter 2: Characterizing Load Flow Feasibility

### 2.1 Load flow

#### 2.1.1 Polar and Rectangular Coordinate Forms

The steady state analysis of a power system is described in terms of a set of non-linear algebraic equations known as the load flow equations. These equations have special properties when expressed in rectangular coordinates. It is their quadratic structure that forms the basis of load flow feasibility analysis [16].

In the standard load flow formulation, load buses are modeled as  $PQ$  buses and generation buses as  $PV$  with one of them taken as the slack bus where the real power injection is not specified. Therefore the nodal bus injections have the following formats.

- $z_i = (P_i, Q_i)$  Corresponds to load buses
- $z_i = (P_i, V_i^2)$  Corresponds to generation buses
- $z_i = (V_i^2)$  Corresponds to the slack bus

It can be shown that injections  $z_i (P_i, Q_i \text{ or } V_i^2)$  are of the quadratic form [11, 12],

$$z_i = \underline{x}^T \underline{J}_i \underline{x} \quad (2.1)$$

where  $\underline{x}$  is the vector of the nodal voltage components in rectangular coordinates  $\underline{x} = (\underline{e}, \underline{f})^T$  and  $\underline{J}_i$  is a  $2N \times 2N$  constant real symmetric matrix, which is uniquely defined by the type of injection and the network admittance matrix (see Section 2.3.2 for a more detailed derivation of the matrices  $\underline{J}_i$ ).

The relation between the injections and the nodal voltages can be derived in polar or rectangular coordinates [14]. The complex bus power injected into node  $i$  has the following form.

$$\begin{aligned} \bar{S}_i &= \bar{V}_i \bar{I}_i^* \\ &= P_i + jQ_i \end{aligned} \quad (2.2)$$

In Equation (2.2):



- $\bar{V}_i$  and  $\bar{I}_i$  are the complex voltage and the current injection at node  $i$
- $P_i$  and  $Q_i$  are the real and reactive power injections at node  $i$

The current  $\bar{I}_i$  can be expressed as

$$\bar{I}_i = \sum_{k=1}^N \bar{V}_k \bar{Y}_{ik} \quad (2.3)$$

where the  $\bar{Y}_{ik}$ s are the elements of the network bus admittance matrix  $\bar{Y}$ . Substituting Equation (2.3) into Equation (2.2) gives

$$\bar{S}_i = \bar{V}_i \sum_{k=1}^N \bar{V}_k^* \bar{Y}_{ik}^* \quad (2.4)$$

In Equation (2.4) the voltage can be expressed in either polar,  $\bar{V}_i = V_i \cdot e^{j\delta_i}$ , or rectangular coordinates,  $\bar{V}_i = e_i + j \cdot f_i$ , and the real and imaginary parts can be extracted to obtain,

$$P_i = V_i \sum_{j=1}^N V_j (G_{ij} \cos \delta_{ij} - B_{ij} \sin \delta_{ij}) \quad (2.5)$$

$$Q_i = V_i \sum_{j=1}^N V_j (G_{ij} \sin \delta_{ij} - B_{ij} \cos \delta_{ij}) \quad (2.6)$$

for polar coordinates, and

$$P_i = \sum_{j=1}^N e_i [G_{ij} e_j - B_{ij} f_j] + f_i [G_{ij} f_j - B_{ij} e_j] \quad (2.7)$$

$$Q_i = \sum_{j=1}^N f_i [G_{ij} e_j - B_{ij} f_j] + e_i [G_{ij} f_j + B_{ij} e_j] \quad (2.8)$$

for rectangular coordinates, where  $G_{ij}$  and  $B_{ij}$  are the real and imaginary parts of the elements of the bus admittance  $\bar{Y}$ . These  $P_i$  and  $Q_i$  formulations of Equations (2.7) and (2.8) together with the  $V_i^2$  definition from the rectangular coordinate formulation of the nodal voltages,

$$V_i^* = e_i^2 + f_i^2 \quad (2.9)$$

define the injections for  $PQ$  and  $PV$  buses. Subsequently, the slack bus injection only includes  $V_N^2$  with the given  $e_N$  and  $f_N$ . Furthermore, the value of  $f_N$  can be set to zero

without loss of generality [4, 11]. This results in a reduction of the dimension of  $\underline{x}$  to  $2N - 1$ , which correspondingly results in simplifying the  $\underline{J}_i$  matrix to  $(2N - 1) \times (2N - 1)$ .

$$\underline{x} = [e_1, e_2, \dots, e_N, f_1, f_2, \dots, f_{N-1}] \quad (2.10)$$

Therefore in a network with  $N$  buses of which  $npq$  are  $PQ$  buses, the bus injections can be defined as a vector of the following form.

$$\underline{z} = [P_1, Q_1, \dots, P_{npq}, Q_{npq}, P_{npq+1}, V_{npq+1}^2, \dots, P_{N-1}, V_{N-1}^2, V_N^2] \quad (2.11)$$

This Equation (2.11) can be put into a more general form using Equations (2.7) and (2.8).

$$\begin{aligned} \underline{z} &= \begin{bmatrix} \underline{x}^T \underline{J}_1 \\ \underline{x}^T \underline{J}_2 \\ \vdots \\ \underline{x}^T \underline{J}_i \\ \vdots \\ \underline{x}^T \underline{J}_{2N} \end{bmatrix} \\ &= \underline{L}(\underline{x}) \underline{x} \end{aligned} \quad (2.12)$$

Additionally, it can be shown that  $\underline{L}(\underline{x})$  is half of the Jacobian matrix by taking the first derivative of  $\underline{z} = \underline{L}(\underline{x}) \underline{x}$  with respect to  $\underline{x}$  which gives

$$\frac{\delta \underline{z}}{\delta \underline{x}} = 2 \underline{L}(\underline{x}) \quad (2.13)$$

where  $\frac{\delta \underline{z}}{\delta \underline{x}}$  is the Jacobian of the load flow equation [6].

### 2.1.2 Hand solved example

It is helpful to illustrate the above theory through a simple 2-bus network consisting of a slack bus 1 and a  $PQ$  bus 2 connected through a line with impedance  $jX_l$  as shown in Figure 2-1.

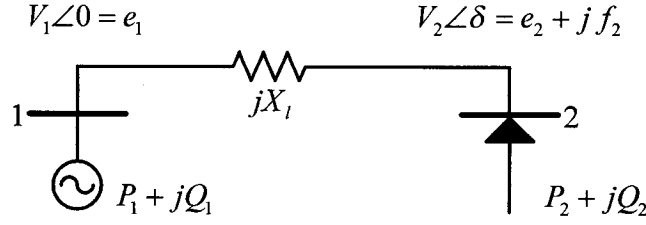


**Figure 2-1:** 2-bus network example with one  $PQ$  bus

As discussed in the previous section, the voltage at bus 1 has only the real part  $e_1$  since it is the reference bus. According to Equation (2.2), the complex power injection into bus 2 is,

$$\begin{aligned}\bar{S}_2 &= \bar{V}_2 (\bar{I}_2^*) \\ &= P_2 + jQ_2\end{aligned}\quad (2.14)$$

Therefore,

$$\begin{aligned}P_2 + jQ_2 &= \bar{V}_2 \left[ \frac{(\bar{V}_2 - \bar{V}_1)}{jX_l} \right]^* \\ &= \bar{V}_2 \left[ \frac{\bar{V}_2^*}{-jX_l} + \frac{-\bar{V}_1^*}{-jX_l} \right] \\ &= j \left[ \frac{\bar{V}_2 \bar{V}_2^*}{X_l} - \frac{\bar{V}_2 \bar{V}_1^*}{X_l} \right]\end{aligned}\quad (2.15)$$

Equation (2.15) can be further expanded, using the polar and rectangular definitions of  $\bar{V}_1$  and  $\bar{V}_2$ .

In the case of polar coordinates,

$$\bar{V}_i = V_i \cdot e^{j\delta_i} \quad (2.16)$$

Equation (2.15) becomes,

$$\begin{aligned}P_2 + jQ_2 &= j \left[ \frac{V_2^2}{X_l} - \frac{V_1 V_2 \cos \delta - j V_1 V_2 \sin \delta}{X_l} \right] \\ &= \frac{V_1 V_2 \sin \delta}{X_l} + j \left[ \frac{V_2^2 - V_1 V_2 \cos \delta}{X_l} \right]\end{aligned}\quad (2.17)$$

Therefore the real and imaginary parts of the transferred power are as following.

$$\begin{aligned}
P_2 &= \frac{V_1 V_2}{X_l} \sin \delta \\
Q_2 &= \frac{V_2^2 - V_1 V_2 \cos \delta}{X_l}
\end{aligned} \tag{2.18}$$

On the other hand, using the rectangular coordinate definition for the bus voltages,

$$\bar{V}_i = e_i + j \cdot f_i \tag{2.19}$$

the current  $\bar{I}_2$  in Equation (2.14) can be expressed as

$$\begin{aligned}
\bar{I}_2 &= \frac{\bar{V}_2 - \bar{V}_1}{jX_l} \\
&= \frac{1}{jX_l} [(e_2 - e_1) + jf_2]
\end{aligned} \tag{2.20}$$

Therefore the injection at bus 2 is,

$$\begin{aligned}
P_2 + jQ_2 &= \bar{V}_2 \bar{I}^* \\
&= (e_2 + jf_2) \left(-\frac{1}{jX_l}\right) [(e_2 - e_1) - jf_2] \\
&= \frac{1}{X_l} [e_2 f_2 - f_2 (e_2 - e_1)] + j \frac{1}{X_l} [f_2^2 + e_2 (e_2 - e_1)]
\end{aligned} \tag{2.21}$$

from which the real and imaginary parts can be extracted.

$$\begin{aligned}
P_2 &= \frac{1}{X_l} e_1 f_2 \\
Q_2 &= \frac{1}{X_l} (-e_1 e_2 + e_2^2 + f_2^2)
\end{aligned} \tag{2.22}$$

Therefore, if the vector of nodal voltages  $\underline{x}$  is defined as,

$$\underline{x} = \begin{bmatrix} e_1 \\ e_2 \\ f_2 \end{bmatrix} \tag{2.23}$$

then the vector of injections  $\underline{z}$  is as follows.

$$\underline{z} = \begin{bmatrix} P_2 \\ Q_2 \\ V_1^2 \end{bmatrix} = \begin{bmatrix} \frac{e_1 f_2}{X_l} \\ \frac{(-e_1 e_2 + e_2^2 + f_2^2)}{X_l} \\ e_1^2 + f_1^2 \end{bmatrix} \quad (2.24)$$

## 2.2 Feasibility Region

### 2.2.1 Feasibility Region $R_z$

Load flow feasibility is concerned with those conditions on the specified power and voltage magnitude injections under which a steady state equilibrium is physically possible. These limitations on the specified injections are imposed by the network structure, that is,

- The nature of the bus types
- The bus admittance matrix

Mathematically, this problem is equivalent to those conditions characterizing the set of nonlinear load flow equations for which a real voltage solution can exist.

The complete characterization of the load flow feasibility can be conceptually addressed through a set  $R_z$  [6]. This set is defined in the space of injections and is called the load flow feasibility or steady state stability region. The set  $R_z$  characterizes all injections  $\underline{z}$ , for which a real solution  $\underline{x}$  to the load flow problem exists,

$$R_z = \left\{ \underline{z} \mid \underline{z} = L(\underline{x})\underline{x}, \underline{x} \in R^{2N-1} \right\} \quad (2.25)$$

where the dimension of  $\underline{x}$  is reduced to  $2N-1$ , without loss of generality by setting  $f_N = 0$  as discussed in section 2.1.1.

One can explicitly characterize the load flow feasibility region  $R_z$  by exploiting the quadratic nature of the load flow equations in rectangular coordinates [11, 12, 13]. The following characteristics of  $R_z$ , result from these quadratic properties.

Region  $R_z$  is a cone stretching to infinity whose vertex is at the origin of the space of injections. This is shown in Figure 2-2 for a simple network with 3-dimensional injections.

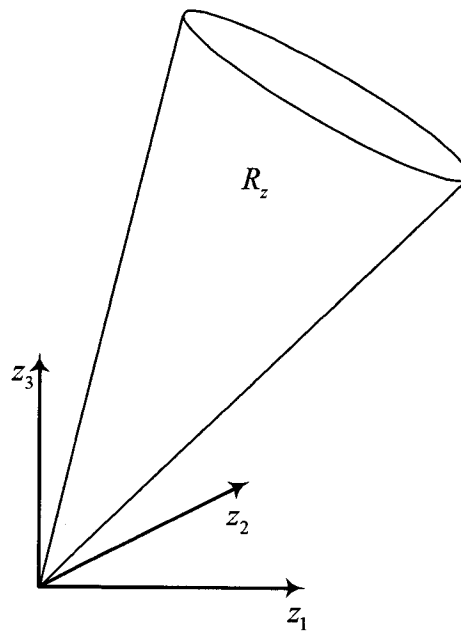


**Figure 2-2:** Feasibility region  $R_z$  of a 3-dimensional injection space

Region  $R_z$  lies above a set of supporting hyperplanes all passing through the origin. These hyperplanes are of the form  $\underline{\alpha}^T \underline{z} = 0$  and will be discussed in more detail in section (2.3.1).

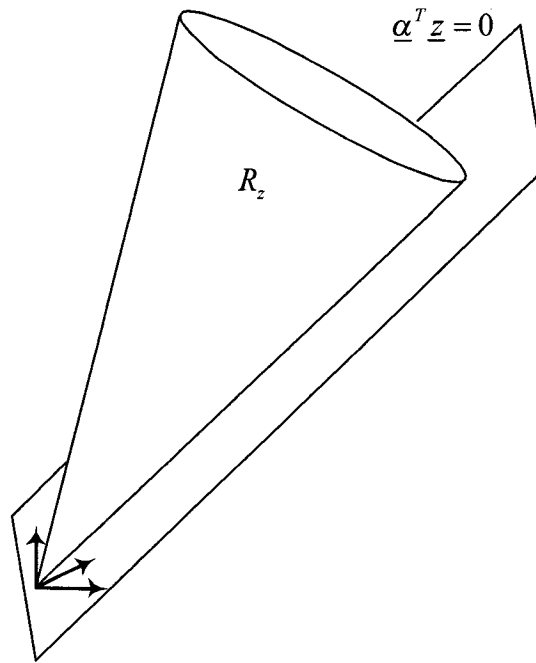


**Figure 2-3:** Feasibility region lies above a set of hyperplanes

### 2.2.2 Feasibility Region on a Plane

To analyze the feasibility region  $R_z$ , it is useful to consider the intersection between the feasibility region  $R_z$  and a plane  $\underline{z}_0^T \underline{z} = k$  with normal vector  $\underline{z}_0$ . The set of  $\underline{z}$  belonging to this intersection is called the feasibility region on a plane and given the symbol  $P_{z_0}$ .

$$P_{z_0} = R_z \cap \{ \underline{z} \mid \underline{z}_0^T \underline{z} = k \} \quad (2.26)$$

Such an intersection is shown in Figures 2-4 (a) and 2-4 (b) where a plane cuts  $R_z$  in a three dimensional setting.

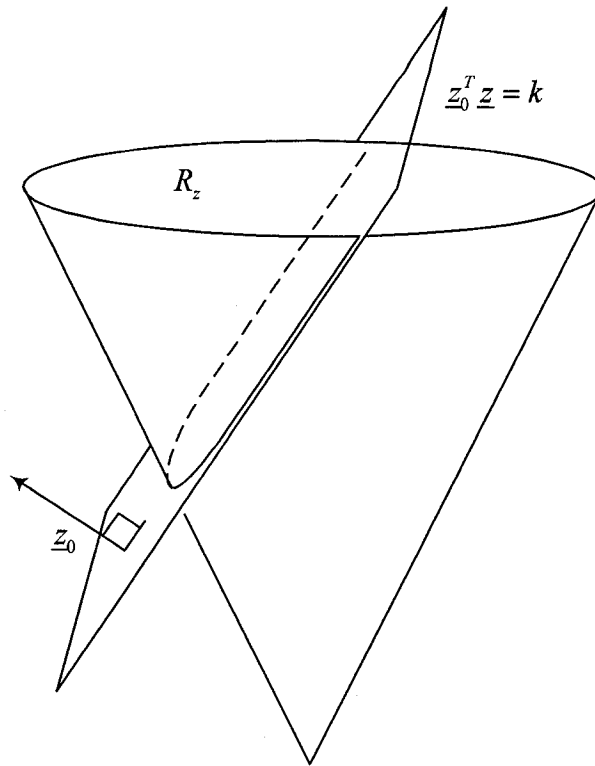


**Figure 2-4 (a):** Geometrical illustration of feasibility region on a plane  $P_{z_0}$  (the plane  $z_0^T z = k$  does not intersect all rays in  $R_z$ )

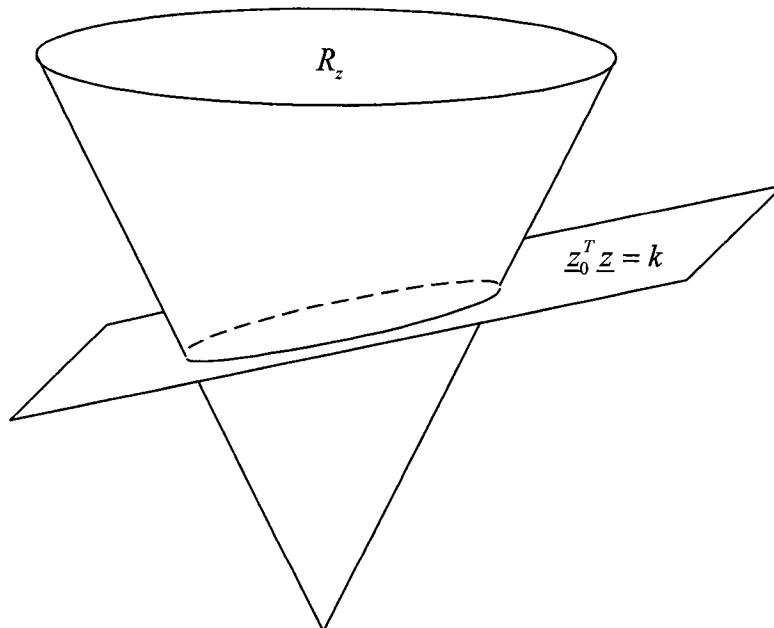


**Figure 2-4 (b):** Geometrical illustration of feasibility region on a plane  $P_{z_0}$  (the plane  $z_0^T z = k$  intersects all rays in  $R_z$ )



In Figure 2-4 (b), the set  $P_{z_0}$  cuts all the rays of  $R_z$  at some finite length. This implies that for all  $z \in R_z$ ,  $z_0^T z \geq 0$ . The plane  $z_0^T z = k \geq 0$  cuts all the rays in  $R_z$  if and only if the matrix  $J(z_0)$  is positive definite [6]. The  $J$  matrix and its formulation are discussed in section (2.3.2). From experience, a suggested value of  $z_0$  that would intersect all rays in  $R_z$  is given by

- $z_0(V^2) = 1.0$  the element of  $z_0$  corresponding to the voltage injection
- $z_0(P) = 0.0$  the element of  $z_0$  corresponding to the real power injection
- $z_0(Q) = 0.1$  the element of  $z_0$  corresponding to the reactive power injection

### 2.2.3 Hand solved example to illustrate notion of feasibility region on a plane

It is helpful to look at the example of the 2-bus network discussed in section (2.1.2). In order to visualize the feasibility region on a plane, first consider the terms  $P_2$  and  $Q_2$  of the injection vector  $z_g$ . Their polar coordinates formulation as seen in Equation (2.18) is,

$$\begin{aligned} P_2 &= \frac{V_1 V_2}{X_l} \sin \delta \\ Q_2 &= \frac{V_2^2 - V_1 V_2 \cos \delta}{X_l} \end{aligned} \quad (2.27)$$

In section 1.2, the exact feasibility region was defined using the following inequality,

$$V_1^4 + 4 V_1^2 X_l Q_2 - 4 X_l^2 P_2^2 \geq 0 \quad (2.28)$$

The graph of (2.28) is shown in the space of  $P_2$ ,  $Q_2$  and  $V_1^2$  in Figure 2-5.

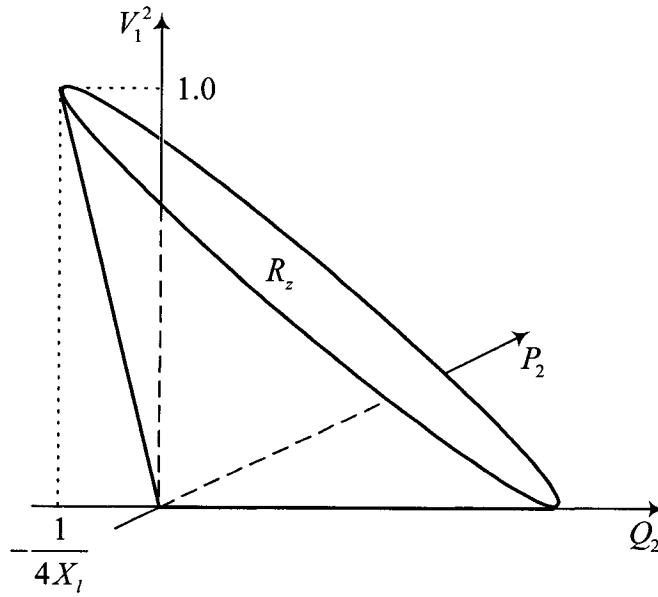


**Figure 2-5:** Load flow feasibility region  $R_z$  of the network in Figure 2-1

Cutting this feasibility region with a plane  $\underline{z}_0^T \underline{z} = k$  where,

$$\underline{z}_0 = \begin{bmatrix} P_2 \\ Q_2 \\ V_1^2 \end{bmatrix} = \begin{bmatrix} 0 \\ 0 \\ 1 \end{bmatrix}$$

results in the following graph,

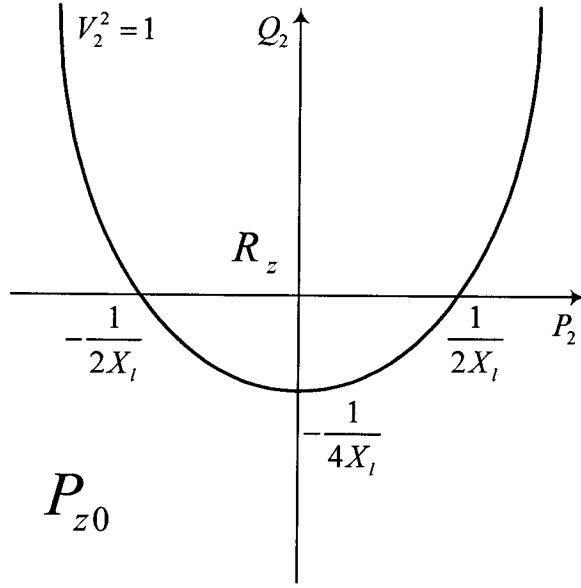


**Figure 2-6:** Feasibility region on a plane  $P_{z_0}$  (the plane  $\underline{z}_0^T \underline{z} = k$  does not intersect all rays in  $R_z$ )

As seen in Figure 2-6, the plane  $\underline{z}_0^T \underline{z} = k$  does not cut all the rays in  $R_z$ , hence the intersection is not a closed surface.

Now, if we assume an intersecting plane with  $\underline{z}_0$  as suggested in section 2.2.2,

$$\underline{z}_0 = \begin{bmatrix} 0 \\ 0.1 \\ 1 \end{bmatrix}$$

The intersecting plane  $\underline{z}_0^T \underline{z} = k$  is therefore defined by,

$$V_1^2 + 0.1Q_2 = k$$

which combined with equation (2.28) yields the feasibility region on a plane as,

$$(k - 0.1 Q_2)^2 + 4(k - 0.1 Q_2) X_1 Q_2 - 4X_1 P_2^2 \geq 0 \quad (2.29)$$

By rearranging Equation (2.29), we obtain,

$$k^2 + (4kX_1 - 0.2k) Q_2 + (-0.01 - 0.4X_1) Q_2^2 - 4X_1 P_2^2 \geq 0 \quad (2.30)$$

Further simplification of Equation (2.30) results in the following,

$$d + c Q_2 + \frac{Q_2^2}{a^2} + \frac{P_2^2}{b^2} \leq 0 \quad (2.31)$$

where,

$$a = \frac{1}{(0.01 + 0.4X_1)}$$

$$b = \frac{1}{(4X_1)}$$

$$c = (0.2k - 4kX_1)$$

$$d = -k^2$$

$$K = d - \frac{a^2 c^2}{4}$$

Completing the square results in the following equation,

$$\frac{1}{a^2} \left( Q_2 + \frac{a^2 c}{2} \right)^2 + \frac{1}{b^2} P_2^2 = K^2 \quad (2.32)$$

which is the equation of an ellipse as shown in Figure 2-7.

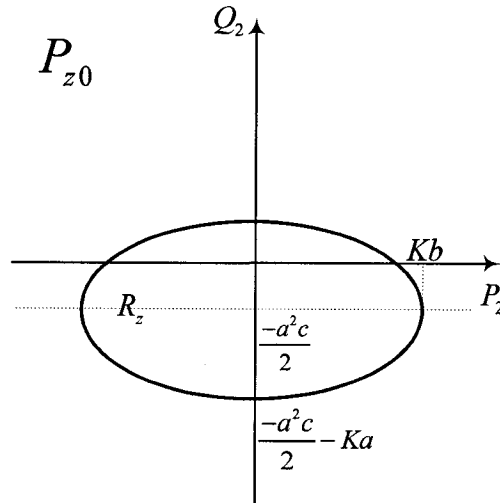


**Figure 2-7:** Feasibility region on a plane  $P_{z_0}$  (the plane  $\underline{z}_0^T \underline{z} = k$  intersects all rays in  $R_z$ )

It can be seen that the above choice of  $\underline{z}_0$  results in a set  $P_{z_0}$  which intersects all rays in  $R_z$ .

## 2.3 Supporting Hyperplanes

### 2.3.1 Definition and Solution Method

As suggested in section (2.2.1), the feasibility region  $R_z$  has a set of supporting hyperplanes (SH) of the form  $\underline{\alpha}^T \underline{z} = 0$ . Such hyperplanes are graphically shown in Figure 2-8 (a) where the  $\underline{z}_b$ s are the intersection points of the feasibility region with the hyperplanes. Figure 2-8 (b) shows the SH with respect to the feasibility region on a plane  $P_{z_0}$  where we see that given enough such SH, the set  $P_{z_0}$  could be approximately characterized.

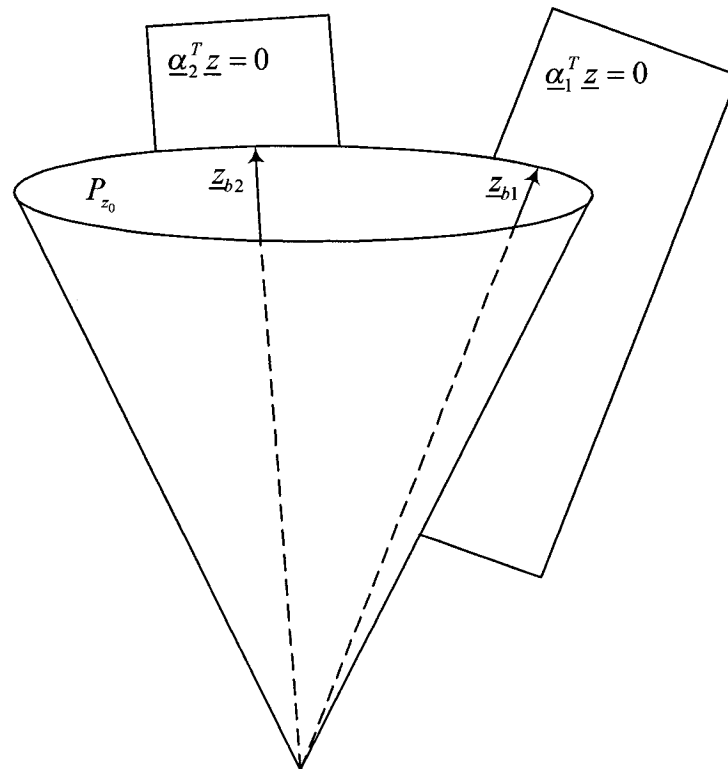


**Figure 2-8 (a):** Example of supporting hyperplanes  $\underline{\alpha}^T \underline{z} = 0$  of the load flow feasibility region  $R_z$

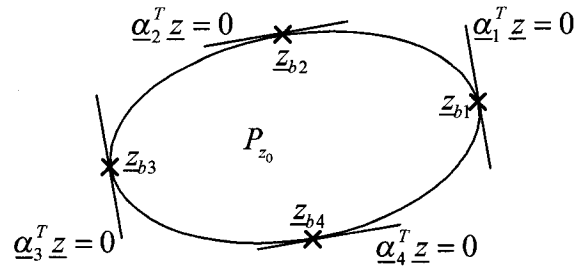


**Figure 2-8 (b):** 2-dimensional feasibility surface  $P_{z_0}$

A supporting hyperplane  $\underline{\alpha}^T \underline{z} = 0$  can be found by searching over the feasibility region on a plane  $P_{z_0}$  in some arbitrary search direction  $\underline{z}_1$  such that  $\underline{z}_1 \neq \underline{z}_0$  and  $\underline{z}_1 \neq -\underline{z}_0$ . This search direction vector  $\underline{z}_1$  defines a plane  $\underline{z}_1^T \underline{z} = c$  which intersects the set  $P_{z_0}$  for different values of  $c$ . As shown in Figures 2-9 (a) and 2-9 (b), by varying  $c$ , the finite minimum and maximum values of  $c$  over  $P_{z_0}$  can be obtained.

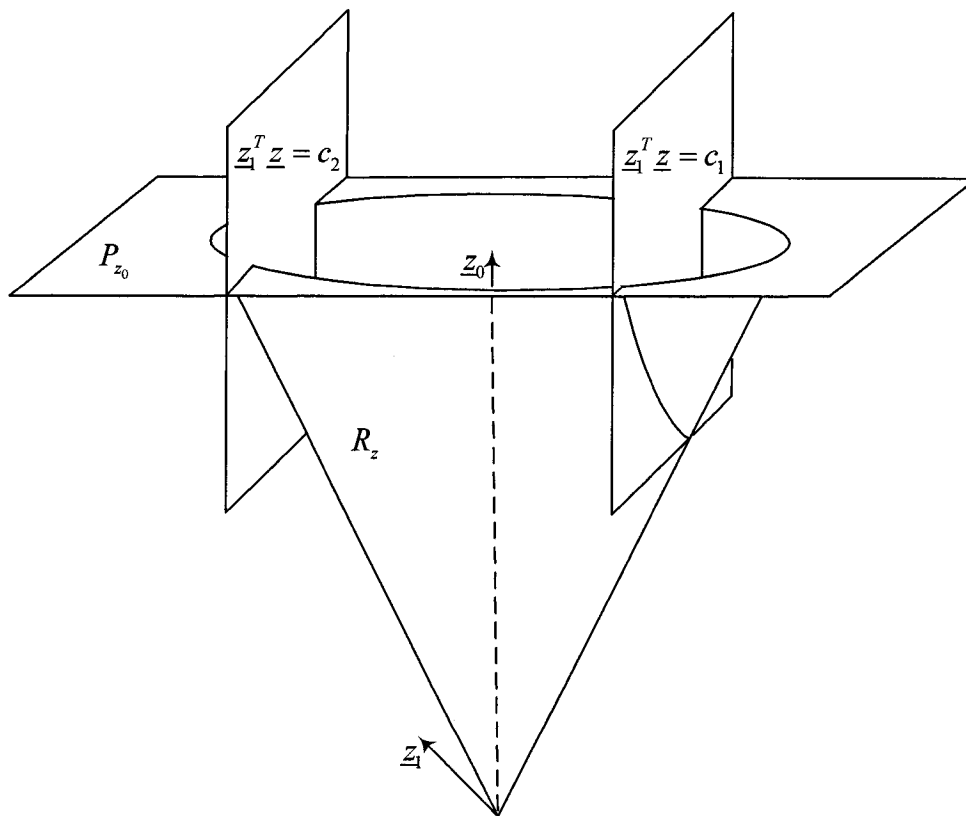


**Figure 2-9 (a):** Intersection of the plane  $\underline{z}_1^T \underline{z} = c$  with  $P_{z_0}$  for various values of  $c$ .

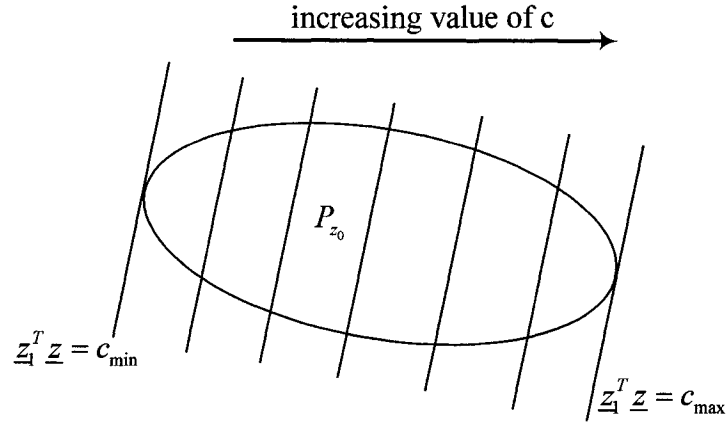


**Figure 2-9 (b):** Intersection of the plane  $\underline{z}_1^T \underline{z} = c$  with  $P_{z_0}$  for various values of  $c$ .

The search for the arbitrary supporting hyperplane,  $\underline{\alpha}^T \underline{z} = 0$ , can be formulated as an optimization

$$\begin{aligned} \max_{\underline{z} \in R_z} \quad & \underline{z}_1^T \underline{z} = c \\ \text{s.t.} \quad & \\ & \underline{z}_0^T \underline{z} = k \end{aligned} \quad (2.33)$$

This optimization can be simplified using the following identities (2.34) and (2.35) to obtain the eigenvalue problem (2.36)

$$\underline{z}_1^T \underline{z} = \underline{x}^T J(\underline{z}_1) \underline{x} \quad (2.34)$$

$$\underline{z}_0^T \underline{z} = \underline{x}^T J(\underline{z}_0) \underline{x} \quad (2.35)$$

$$[J(\underline{z}_1) - \lambda J(\underline{z}_0)] \underline{x} = \underline{0} \quad (2.36)$$

Equation (2.36) results in a set of real eigenvalues  $\underline{\lambda}$  and their corresponding eigenvectors. The maximum and minimum such eigenvalues then define the corresponding hyperplanes according to the following expressions (2.37) and (2.38) [6],

$$\underline{\alpha} = (\lambda_{\max} \underline{z}_0 - \underline{z}_1) \quad \lambda = \lambda_{\max} \quad (2.37)$$

$$\underline{\alpha} = (\underline{z}_1 - \lambda_{\min} \underline{z}_0) \quad \lambda = \lambda_{\min} \quad (2.38)$$

This eigenvalue problem is at the core of the supporting hyperplane method since the maximum or minimum eigenvalues result in the  $\alpha$ 's which define the supporting hyperplanes. Moreover, the corresponding eigenvectors solving equation (2.36) become

the nodal voltages  $\underline{x}_b$  corresponding to the injection at the boundary of the feasibility region where the SH is tangent to  $R_z$ .

### 2.3.2 J-Matrix Implementation

Consider a network with the following bus information

- $N$  Total number of buses
- $npq$  Number of  $PQ$  buses
- $npv$  Number of  $PV$  buses excluding the slack  $npv = N - npq - 1$

The injections are now written in the following format

$$\underline{z} = \begin{bmatrix} \underline{P} \\ \underline{Q} \\ \underline{V}^2 \end{bmatrix} \leftarrow \begin{matrix} N-1 \\ npq \\ npv+1 \end{matrix} \quad (2.39)$$

$$\underline{x} = \begin{bmatrix} \underline{e} \\ \underline{f} \end{bmatrix} \leftarrow \begin{matrix} N \\ N-1 \end{matrix} \quad (2.40)$$

Both of these vectors have  $2N-1 \times 1$  dimensions. Furthermore, if  $\underline{\alpha}$  is a constant injection vector of dimensions  $2N-1 \times 1$ ,

$$\underline{\alpha} = \begin{bmatrix} \underline{\alpha}_P \\ \underline{\alpha}_Q \\ \underline{\alpha}_{V^2} \end{bmatrix} \quad (2.41)$$

then,

$$\underline{\alpha}^T \begin{bmatrix} \underline{P} \\ \underline{Q} \\ \underline{V}^2 \end{bmatrix} = \underline{\alpha}_P^T \underline{P} + \underline{\alpha}_Q^T \underline{Q} + \underline{\alpha}_{V^2}^T \underline{V}^2 \quad (2.42)$$

The  $\underline{\alpha}_P^T \underline{P}$  element on the right hand side of Equation (2.42) can be expressed as

$$\underline{\alpha}_P^T \underline{P} = [\underline{e}^T \quad \underline{f}^T] J(\underline{\alpha}_P) \begin{bmatrix} \underline{e}^T \\ \underline{f}^T \end{bmatrix} \quad (2.43)$$

where, recalling that  $z_i = \underline{x}^T J_i \underline{x}$ , we define



$$\underline{\alpha}^T \underline{z} \triangleq \underline{x}^T \underline{J}(\underline{\alpha}) \underline{x} \quad (2.44)$$

with  $J(\alpha) = \sum_{i=1}^{2nb-1} \alpha_i J_i$ .

The specific nature of  $J(\alpha) = \sum_{i=1}^{2nb-1} \alpha_i J_i$  can be derived as follows. We begin with Equation (2.7) showing the relation between the real power injection at bus  $i$  and the complex voltages in rectangular coordinates

$$P_i = \sum_{j=1}^N e_i [G_{ij} e_j - B_{ij} f_j] + f_i [G_{ij} f_j - B_{ij} e_j] \quad (2.45)$$

This can be expressed in matrix format as

$$\underline{P} = \text{diag}(\underline{e}) [\underline{G} \underline{e} - \underline{B} \underline{f}] + \text{diag}(\underline{f}) [\underline{G} \underline{f} - \underline{B} \underline{e}] \quad (2.46)$$

where  $\text{diag}(\underline{e})$  is a diagonal matrix with elements of  $\underline{e}$  on its diagonal. The right hand side of Equation (2.46) can be separated into four terms.

$$\begin{cases} \text{diag}(\underline{e}) \underline{G} \underline{e} \\ \text{diag}(\underline{e}) (-\underline{B}) \underline{f} \\ \text{diag}(\underline{f}) \underline{G} \underline{e} \\ \text{diag}(\underline{f}) (-\underline{B}) \underline{f} \end{cases}$$

The first term,  $\text{diag}(\underline{e}) \times \underline{G} \times \underline{e}$  can be used to write Equation (2.35) as,

$$\begin{aligned} \underline{\alpha}_p^T \underline{P} &= \underline{\alpha}_p^T [\text{diag}(\underline{e}) \underline{G} \underline{e}] \\ &= \underline{e}^T [\text{diag}(\underline{\alpha}_p) \underline{G} \underline{e}] \end{aligned} \quad (2.47)$$

Furthermore, one can use Equation (2.47) and the following matrix identity

$$\underline{e}^T \underline{A} \underline{e} = \underline{e}^T \left( \frac{\underline{A} + \underline{A}^T}{2} \right) \underline{e} \quad (2.48)$$

to express Equation (2.43) in terms of a symmetric J-matrix,

$$\underline{e}^T \left[ \frac{\text{diag}(\underline{\alpha}_p) \underline{G} + \underline{G} \text{diag}(\underline{\alpha}_p)}{2} \right] \underline{e} \quad (2.49)$$

The same technique can be used to expand the three other terms on the right hand side of Equation (2.46) to obtain a general format for  $\underline{J}(\underline{\alpha}_p)$ ,

$$\underline{J}(\underline{\alpha}_p) = \frac{1}{2} \begin{bmatrix} \text{diag}(\underline{\alpha}_p) \underline{G} + \underline{G} \text{diag}(\underline{\alpha}_p) & \underline{B} \text{diag}(\underline{\alpha}_p) - \text{diag}(\underline{\alpha}_p) \underline{B} \\ \text{diag}(\underline{\alpha}_p) \underline{B} - \underline{B} \text{diag}(\underline{\alpha}_p) & \text{diag}(\underline{\alpha}_p) \underline{G} + \underline{G} \text{diag}(\underline{\alpha}_p) \end{bmatrix} \quad (2.50)$$

and similarly for  $\underline{J}(\underline{\alpha}_Q)$  and  $\underline{J}(\underline{\alpha}_{V^2})$

$$\underline{J}(\underline{\alpha}_Q) = \frac{1}{2} \begin{bmatrix} -\text{diag}(\underline{\alpha}_Q) \underline{B} - \underline{B} \text{diag}(\underline{\alpha}_Q) & \underline{G} \text{diag}(\underline{\alpha}_Q) - \text{diag}(\underline{\alpha}_Q) \underline{G} \\ \text{diag}(\underline{\alpha}_Q) \underline{G} - \underline{G} \text{diag}(\underline{\alpha}_Q) & -\text{diag}(\underline{\alpha}_Q) \underline{B} - \underline{B} \text{diag}(\underline{\alpha}_Q) \end{bmatrix} \quad (2.51)$$

$$\underline{J}(\underline{\alpha}_{V^2}) = \begin{bmatrix} \text{diag}(\underline{\alpha}_{V^2}) & 0 \\ 0 & \text{diag}(\underline{\alpha}_{V^2}) \end{bmatrix} \quad (2.52)$$

Finally,  $\underline{J}(\underline{\alpha})$  can be constructed as the sum of the three components in Equations (2.50), (2.51) and (2.52)

$$\underline{\alpha}^T \begin{bmatrix} \underline{P} \\ \underline{Q} \\ \underline{V}^2 \end{bmatrix} = [\underline{e}^T \quad \underline{f}^T] [J(\underline{\alpha}_p) + J(\underline{\alpha}_Q) + J(\underline{\alpha}_{V^2})] \begin{bmatrix} \underline{e}^T \\ \underline{f}^T \end{bmatrix} \quad (2.53)$$

where

$$J(\underline{\alpha}) = J(\underline{\alpha}_p) + J(\underline{\alpha}_Q) + J(\underline{\alpha}_{V^2})$$

### 2.3.3 Hand solved example of the J-matrix and supporting hyperplanes

Consider the previous 2-bus network example depicted in Figure 2-10 with a slack bus 1 and a PQ bus 2 connected through a line with impedance  $jX_l$ .

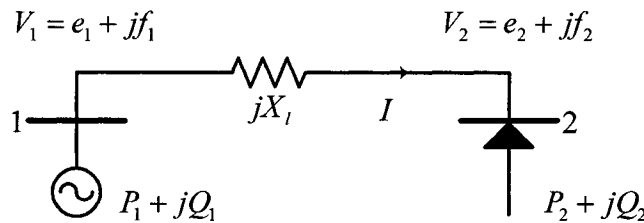


**Figure 2-10:** 2-Bus network example with one PQ bus

In section (2.1.2), it was shown that with the nodal voltage vector  $\underline{x}$  defined as,

$$\underline{x} = \begin{bmatrix} e_1 \\ e_2 \\ f_2 \end{bmatrix} \quad (2.54)$$

and the injection vector  $\underline{z}$  of the form,

$$\underline{z} = \begin{bmatrix} P_2 \\ Q_2 \\ V_1^2 \end{bmatrix} \quad (2.55)$$

then,

$$P_2 = \frac{1}{X_l} e_1 f_2 \quad (2.56)$$

$$Q_2 = \frac{1}{X_l} (-e_1 e_2 + e_2^2 + f_2^2) \quad (2.57)$$

$$V_1^2 = e_1^2 \quad (2.58)$$

In the quadratic format these become,

$$P_2 = \frac{1}{2X_l} \underline{x}^T \underbrace{\begin{bmatrix} 0 & 0 & 1 \\ 0 & 0 & 0 \\ 1 & 0 & 0 \end{bmatrix}}_{J_{P_2}} \underline{x} \quad (2.59)$$

$$Q_2 = \frac{1}{2X_l} \underline{x}^T \underbrace{\begin{bmatrix} 0 & -1 & 0 \\ -1 & 2 & 0 \\ 1 & 0 & 2 \end{bmatrix}}_{J_{Q_2}} \underline{x} \quad (2.60)$$

$$V_1^2 = \underline{x}^T \underbrace{\begin{bmatrix} 1 & 0 & 0 \\ 0 & 0 & 0 \\ 0 & 0 & 0 \end{bmatrix}}_{J_{V_1^2}} \underline{x} \quad (2.61)$$

where  $\underline{J}_{P_2}$ ,  $\underline{J}_{Q_2}$  and  $\underline{J}_{V_1^2}$  matrices are easily found by inspection due to simplicity of the network. The general approach described above yields the same J-matrices as follows:

The admittance matrix of the network in Figure 2-9 is

$$\underline{\bar{Y}} = \begin{bmatrix} \frac{1}{jX_l} & -\frac{1}{jX_l} \\ -\frac{1}{jX_l} & \frac{1}{jX_l} \end{bmatrix} \quad (2.62)$$

with real and imaginary components

$$\underline{G} = \begin{bmatrix} 0 & 0 \\ 0 & 0 \end{bmatrix} \quad (2.63)$$

$$\underline{B} = \frac{1}{X_l} \begin{bmatrix} -1 & 1 \\ 1 & -1 \end{bmatrix} \quad (2.64)$$

To find  $\underline{J}_{P_2}$ ,  $\underline{J}_{Q_2}$  and  $\underline{J}_{V^2}$ , the corresponding vectors as discussed in Equation (2.41) are,

$$\underline{\alpha}_P = \begin{bmatrix} 0 \\ 1 \end{bmatrix} \quad (2.65)$$

$$\underline{\alpha}_Q = \begin{bmatrix} 0 \\ 1 \end{bmatrix} \quad (2.66)$$

$$\underline{\alpha}_{V^2} = \begin{bmatrix} 1 \\ 0 \end{bmatrix} \quad (2.67)$$

According to Equation (2.50),

$$\underline{J}(\underline{\alpha}_p) = \frac{1}{2} \begin{bmatrix} \underline{0} & \underline{B} \text{diag}(\underline{\alpha}_p) - \text{diag}(\underline{\alpha}_p) \underline{B} \\ \text{diag}(\underline{\alpha}_p) \underline{B} - \underline{B} \text{diag}(\underline{\alpha}_p) & \underline{0} \end{bmatrix} \quad (2.68)$$

where,

$$\underline{B} \text{diag}(\underline{\alpha}_p) = \frac{1}{X_l} \begin{bmatrix} -1 & 1 \\ 1 & -1 \end{bmatrix} \begin{bmatrix} 0 & 0 \\ 0 & 1 \end{bmatrix} = \frac{1}{X_l} \begin{bmatrix} 0 & 1 \\ 0 & -1 \end{bmatrix} \quad (2.69)$$

$$\text{diag}(\underline{\alpha}_p) \underline{B} = \frac{1}{X_l} \begin{bmatrix} -1 & 1 \\ 1 & -1 \end{bmatrix} \begin{bmatrix} 0 & 0 \\ 0 & 1 \end{bmatrix} = \frac{1}{X_l} \begin{bmatrix} 0 & 1 \\ 0 & -1 \end{bmatrix} \quad (2.70)$$

hence from (2.68),

$$\underline{J}_{P_2} = \frac{1}{2X_l} \begin{bmatrix} 0 & 0 & 0 & 1 \\ 0 & 0 & -1 & 0 \\ 0 & -1 & 0 & 0 \\ 1 & 0 & 0 & 0 \end{bmatrix} \quad (2.71)$$

The last step is to eliminate the third row and third column which correspond to the reference voltage component  $f_1$  which is arbitrarily and without loss of generality set to zero. The final result which accords with Equation (2.61) is

$$\underline{J}_{P_2} = \frac{1}{2X_l} \begin{bmatrix} 0 & 0 & 1 \\ 0 & 0 & 0 \\ 1 & 0 & 0 \end{bmatrix} \quad (2.72)$$

Similarly,  $\underline{J}_{Q_2}$  and  $\underline{J}_{V_1^2}$  can be calculated according to Equations (2.51) and (2.52).

Having the J-matrices for all injections, we can now calculate arbitrary supporting SHs of the feasibility region  $R_z$ . First, we calculate  $\underline{J}(\underline{\alpha})$  for an arbitrary vector  $\underline{\alpha}$ .

$$\begin{aligned} \underline{J}(\underline{\alpha}) &= J \left( \begin{bmatrix} \alpha_{P_2} \\ \alpha_{Q_2} \\ \alpha_{V_1^2} \end{bmatrix} \right) \\ &= \underline{J}_{P_2} + \underline{J}_{Q_2} + \underline{J}_{V_1^2} \\ &= \frac{\alpha_{P_2}}{2X_l} \begin{bmatrix} 0 & 0 & 1 \\ 0 & 0 & 0 \\ 1 & 0 & 0 \end{bmatrix} + \frac{\alpha_{Q_2}}{2X_l} \begin{bmatrix} 0 & -1 & 0 \\ -1 & 2 & 0 \\ 0 & 0 & 0 \end{bmatrix} + \alpha_{V_1^2} \begin{bmatrix} 1 & 0 & 0 \\ 0 & 0 & 0 \\ 0 & 0 & 0 \end{bmatrix} \end{aligned} \quad (2.73)$$

Further simplification can be made by renaming  $\frac{\alpha_{P_2}}{\alpha_{Q_2}} \triangleq A$  and  $\frac{2X_l\alpha_{V_1^2}}{\alpha_{Q_2}} \triangleq B$ .

$$\underline{J}(\underline{\alpha}) = \frac{\alpha_{Q_2}}{2X_l} \begin{bmatrix} B & -1 & A \\ -1 & 2 & 0 \\ A & 0 & 2 \end{bmatrix} \quad (2.74)$$

Now, in order to solve the eigenvalue problem (2.36), we need to calculate  $J(\underline{z}_0)$  and  $J(\underline{z}_1)$  where  $\underline{z}_1$  is an arbitrary constant injection vector,

$$\underline{z}_1 = \begin{bmatrix} -1 \\ -0.5 \\ 1 \end{bmatrix}$$

and,

$$\underline{z}_0 = \begin{bmatrix} 0 \\ 0.1 \\ 1 \end{bmatrix}$$

Therefore from (2.74),

$$\underline{J}(\underline{z}_0) = \begin{bmatrix} 1 & -\frac{1}{20X_l} & 0 \\ -\frac{1}{20X_l} & \frac{1}{10X_l} & 0 \\ 0 & 0 & \frac{1}{10X_l} \end{bmatrix} \quad (2.75)$$

while,

$$\underline{J}(\underline{z}_1) = \begin{bmatrix} 1 & \frac{1}{4X_l} & -\frac{1}{2X_l} \\ \frac{1}{4X_l} & -\frac{1}{2X_l} & 0 \\ -\frac{1}{2X_l} & 0 & -\frac{1}{2X_l} \end{bmatrix} \quad (2.76)$$

These two matrices,  $\underline{J}(\underline{z}_0)$  and  $\underline{J}(\underline{z}_1)$ , are both symmetric. Before we proceed any further we need to make sure that  $\underline{J}(\underline{z}_0)$  is positive definite. The eigenvalues of  $\underline{J}(\underline{z}_0)$  are,

$$\begin{aligned} \lambda_1 &= \frac{1}{10X_l} \\ \lambda_{2,3} &= \frac{\frac{1}{2}X_l + \frac{1}{20} \pm \frac{1}{20}\sqrt{100X_l^2 - 20X_l + 2}}{X_l} \end{aligned} \quad (2.77)$$

For line reactance values of  $X_l$  greater than 0.025, all the eigenvalues are positive, in which case  $\underline{J}(\underline{z}_0)$  is positive definite. For values of  $X_l$  less than 0.025, one would have to use a different value of  $\underline{z}_0$  to find a positive definite  $\underline{J}(\underline{z}_0)$ .

Referring to Equation (2.36) the eigenvalue problem is as follows.

$$[J(\underline{z}_1) - \lambda J(\underline{z}_0)]\underline{x} = \underline{0} \quad (2.78)$$

For a line reactance value of  $X_l = 0.5$ , the eigenvalues and their corresponding eigenvectors are as follows.

$$\underline{\lambda} = \begin{bmatrix} -5.75 \\ -5 \\ 2.06 \end{bmatrix}$$

$$\underline{x} = \begin{bmatrix} 0.32 & 0 & 0.98 \\ 0.16 & -2.24 & 0.49 \\ 2.13 & 0 & -0.69 \end{bmatrix}$$

The maximum and minimum eigenvalues, as shown in (2.37) and (2.38), define the  $\underline{\alpha}$  vectors defining two supporting hyperplanes  $\underline{\alpha}^T \underline{z} = 0$ .

$$\underline{\alpha}_{\max} = \begin{bmatrix} 1 \\ 0.71 \\ 1.06 \end{bmatrix} \quad \lambda_{\max} = 2.06$$

$$\underline{\alpha}_{\min} = \begin{bmatrix} -1 \\ 0.8 \\ 6.75 \end{bmatrix} \quad \lambda_{\min} = -5.75$$

Furthermore, the corresponding eigenvectors are the nodal voltages  $\underline{x}$ , at the intersection of these SHs and the feasibility region  $R_z$ .

$$\underline{x}_{\max} = \begin{bmatrix} 0.98 \\ 0.49 \\ -0.69 \end{bmatrix}$$

$$\underline{x}_{\min} = \begin{bmatrix} 0.32 \\ 0.16 \\ 2.13 \end{bmatrix}$$

## 2.4 Closest Boundary Injection

### 2.4.1 Feasibility Margin

The degree of load flow feasibility of a given vector of injections  $\underline{z}_g$  can be expressed by a quantitative measure known as the load flow feasibility or steady state feasibility margin (FM) defined as [6],

$$\begin{aligned} \text{FM} &= \frac{\underline{\alpha}^{*T} \underline{z}_g}{\|\underline{\alpha}^*\| \|\underline{z}_g\|} \\ &= \cos(\theta^*) \end{aligned} \quad (2.79)$$

where  $\underline{\alpha}^*$  is the normal vector defining the closest SH to  $\underline{z}_g$ . This is illustrated in Figure 2-11.

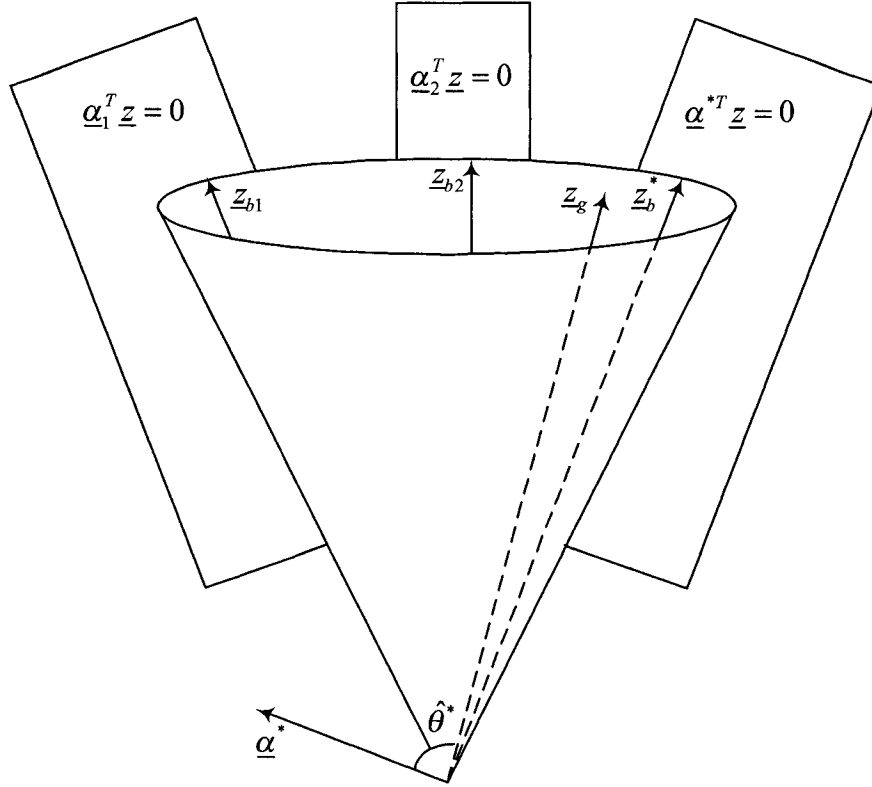


**Figure 2-11:** Geometrical illustration of the feasibility margin FM of a given injection  $\underline{z}_g$

As shown before, the normal vector  $\underline{\alpha}$  can be found from the solution of the generalized eigenvalue problem,

$$[J(\underline{z}_1) - \lambda J(\underline{z}_0)] \underline{x} = \underline{0} \quad (2.80)$$

and it has the form

$$\underline{\alpha} = (\lambda_{\max} \underline{z}_0 - \underline{z}_1) \quad (2.81)$$

or

$$\underline{\alpha} = (\underline{z}_1 - \lambda_{\min} \underline{z}_0) \quad (2.82)$$



where

- $\lambda_{\max}$  and  $\lambda_{\min}$  are the extreme eigenvalues of (2.80)
- $\underline{J}(\underline{z}_0)$  is positive definite.
- $\underline{z}_1$  is an arbitrary search direction.

As long as  $\underline{J}(\underline{z}_0)$  is positive definite, by varying the search direction  $\underline{z}_1$ , all  $\underline{\alpha}$  's belonging to the boundary of  $R_z$  can be found. The boundary injection,  $\underline{z}_b$ , corresponding to such  $\underline{\alpha}$  is,

$$\underline{z}_b = \underline{L}(\underline{x}_b)\underline{x}_b \quad (2.83)$$

where  $\underline{x}_b$  is the eigenvector associated with one of the extreme eigenvalues.

The properties of the steady state FM can be examined by considering its associated closest boundary injection  $\underline{z}_b^*$  given by Equation (2.83).

Pre-multiplying (2.83) by  $\underline{\alpha}^{*T}$ ,

$$\underline{\alpha}^{*T} \underline{z}_b = \underline{\alpha}^{*T} \underline{L}(\underline{x}_b)\underline{x}_b \quad (2.84)$$

and using the identity

$$\underline{\alpha}^T \underline{L}(\underline{x})\underline{x} = \underline{x}^T \underline{J}(\underline{\alpha})\underline{x} \quad (2.85)$$

the following is obtained,

$$\underline{\alpha}^{*T} \underline{z}_b = \underline{x}_b^T \underline{J}(\underline{\alpha}^*)\underline{x}_b \quad (2.86)$$

Writing Equation (2.80) as,

$$\underline{J}(\underline{\alpha})\underline{x}_b = 0 \quad (2.87)$$

then (2.86) becomes

$$\underline{\alpha}^{*T} \underline{z}_b = 0 \quad (2.88)$$

Hence, if a given injection  $\underline{z}_g$  lies on the boundary of  $R_z$  then by Equation (2.79) FM is zero. If however  $\underline{z}_g \in R_z$  then since  $\underline{\alpha}^{*T} \underline{z}_g > 0$ , FM is positive. Otherwise if  $\underline{z}_g \notin R_z$  then since  $\underline{\alpha}^{*T} \underline{z}_g < 0$ , FM is negative.

Here is list of the important characteristics of the feasibility margin of an injection:

- The injection  $\underline{z}_g$  is feasible if and only if  $FM \geq 0$ . This important property can be used independently of the numerical load flow algorithm to test the feasibility of an injection. One can verify whether the non-convergence of a numerical load flow algorithm is due to load flow feasibility violations or to non-convergence of the numerical algorithm.
- Since the FM is defined in terms of the cosine of the angle  $\theta$ , then

$$-1 \leq FM \leq 1$$

Thus, the FM can be used to quantify the degree of feasibility or unfeasibility of a given injection  $\underline{z}_g$ . This allows for a comparison of the load flow feasibility limitations of different network structures.

- In case of load flow feasibility violation, the closest boundary injection associated with the FM can result in a systematic procedure to restore load flow feasibility. This is more efficient than the trial and error method [6].
- The FM can be used to characterize an explicit sufficient load flow feasibility set  $R_s$ . Any injection in  $R_s$  is guaranteed to be feasible. This has potential application in power system security [13].

#### 2.4.2 Optimization Scheme

As discussed in section 2.4.1, the FM is a measure of the degree of feasibility of an injection,  $\underline{z}_g$ , and is defined as,

$$\begin{aligned} FM &= \cos \left( \text{Max}_{\underline{\alpha} \in R_\alpha} \{ \theta \} \right) \\ &= \text{Min}_{\underline{\alpha} \in R_\alpha} \frac{\underline{\alpha}^T \underline{z}_g}{\|\underline{\alpha}\| \|\underline{z}_g\|} \end{aligned} \quad (2.89)$$

where,

- $\theta$  is the angle between  $\underline{\alpha}$  and  $\underline{z}_g$ .
- $R_\alpha$  is the set of normal vectors  $\underline{\alpha}$  defining the supporting hyperplane  $\underline{\alpha}^T \underline{z} = 0$ .

The optimization problem in Equation (2.89) is equivalent to the problem of selecting the closest supporting hyperplane  $\underline{\alpha}^{*T} \underline{z} = 0$  as shown in Figure 2-11. This solution can be formulated as the following.

$$\begin{aligned} \text{FM} &= \cos(\theta^*) \\ &= \frac{\underline{\alpha}^{*T} \underline{z}_g}{\|\underline{\alpha}^*\| \|\underline{z}_g\|} \end{aligned} \quad (2.90)$$

where  $\theta^*$  is the angle between  $\underline{z}_g$  and  $\underline{\alpha}^*$ . Once this solution (2.90) is found, the closest boundary injection  $\underline{z}_b^*$  to  $\underline{z}_g$  can also be found, from which other measures of feasibility such as the minimum Euclidian distance to  $\underline{z}_g$ , can be derived.

This optimization can be implemented using MATLAB. First, there is a program that calculates the normal vector  $\underline{\alpha}$  using the generalized eigenvalue problem,

$$[J(\underline{z}_1) - \lambda J(\underline{z}_0)] \underline{x} = \underline{0} \quad (2.91)$$

In Equation (2.91),  $\underline{z}_0$  is the normal vector as defined in section 2.2.2 and  $\underline{z}_1$  is a given search direction. The resulting  $\underline{\alpha}$  defines the supporting hyperplane corresponding to the direction of  $\underline{z}_1$ , from which the boundary injection  $\underline{z}_b$  can be found. Subsequently, using the calculated  $\underline{\alpha}$  and the given injection  $\underline{z}_g$  the FM corresponding to the search direction can be obtained. The flowchart of this program is shown in Figure 2-12.

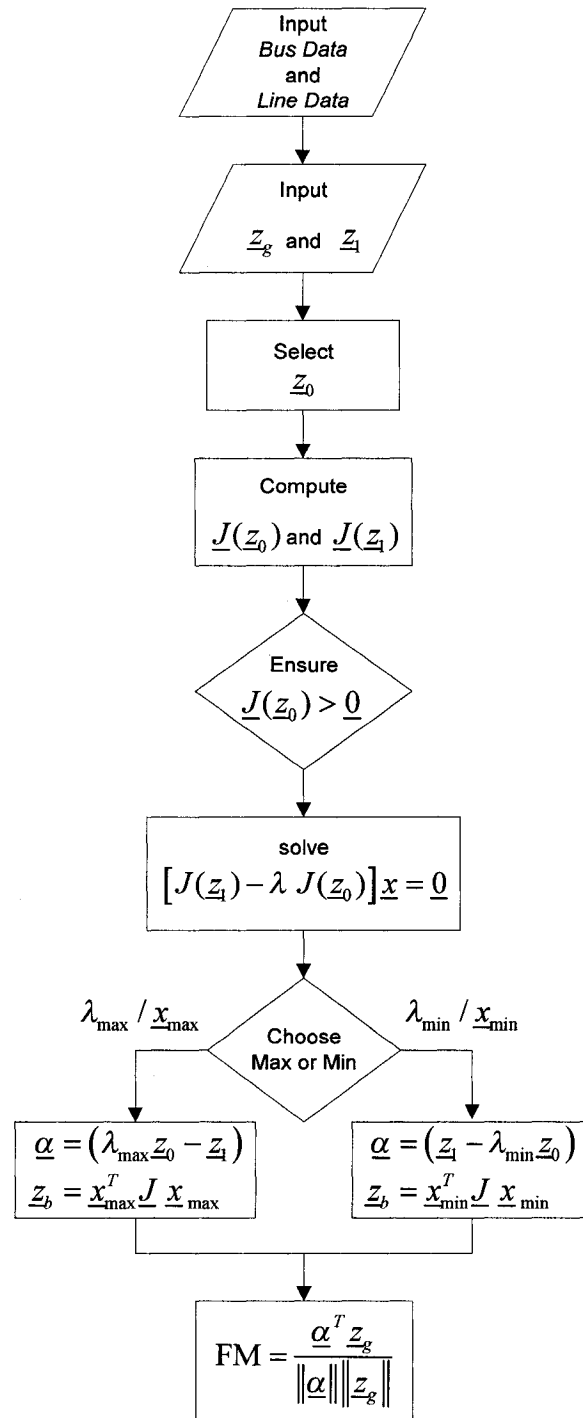


**Figure 2-12:** Flowchart of the program computing feasibility margin

The program begins with the bus and line data of the network to find the admittance matrix  $\bar{Y}$ . The vector  $z_0$  is selected that makes  $\underline{J}(z_0)$  positive definite. The program then computes  $\underline{J}(z_1)$  for an initial guess  $z_1$ . These two matrices are then used to form

the eigenvalue problem, which is solved using MATLAB's  $\text{eig}(A, B)$  function, giving the extreme eigenvalues and their corresponding eigenvectors.

The next step is to select one of the extreme eigenvectors to find the corresponding boundary injection  $\underline{z}_b$ , as well as the  $\underline{\alpha}$  vector defining the boundary hyperplane and the FM.

The steps discussed above can only find an arbitrary boundary injection  $\underline{z}_b$  and corresponding FM given an arbitrary search direction. Hence another program is required to find the best search direction which results in the closest boundary injection. This search process is graphically shown in Figures 2-13 (a) and 2-13 (b).

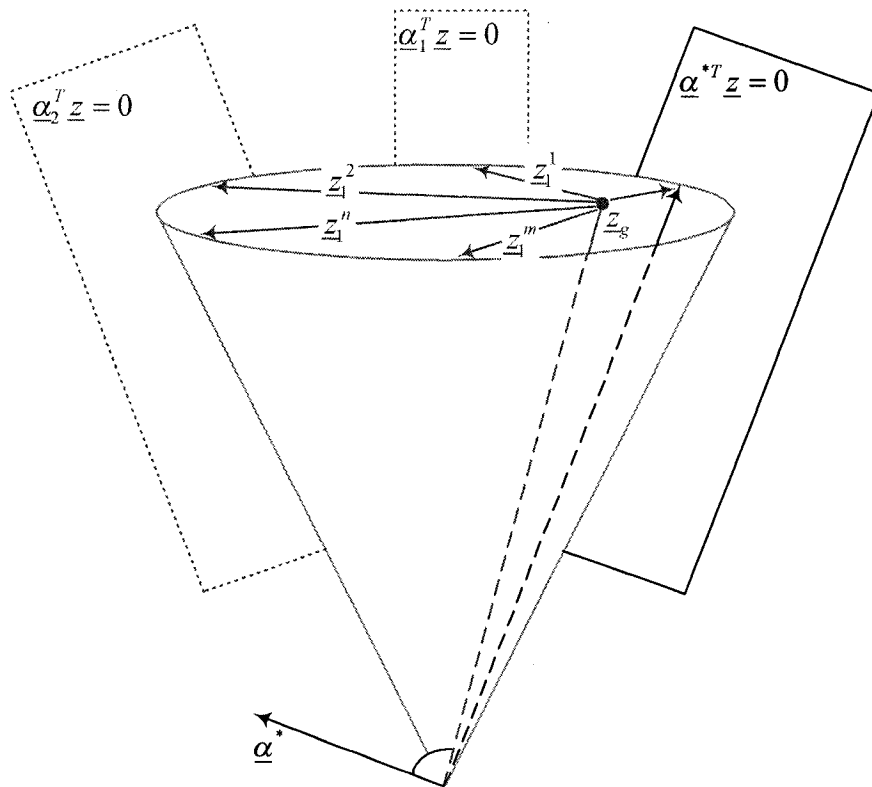


**Figure 2-13 (a):** Illustration of the search process for the closest boundary injection  $\underline{z}_b^*$

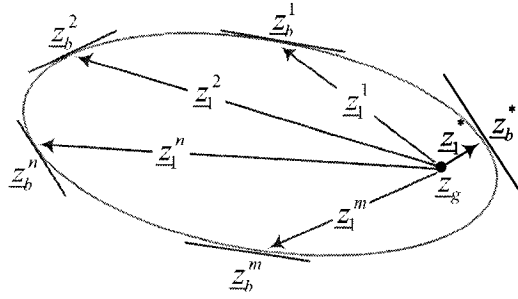


**Figure 2-13 (b):** 2-dimensional feasibility surface  $P_{z_0}$

The second MATLAB program described in Figure 2-14 is an optimization routine to find the search direction which results in the closest boundary point to the given injection.

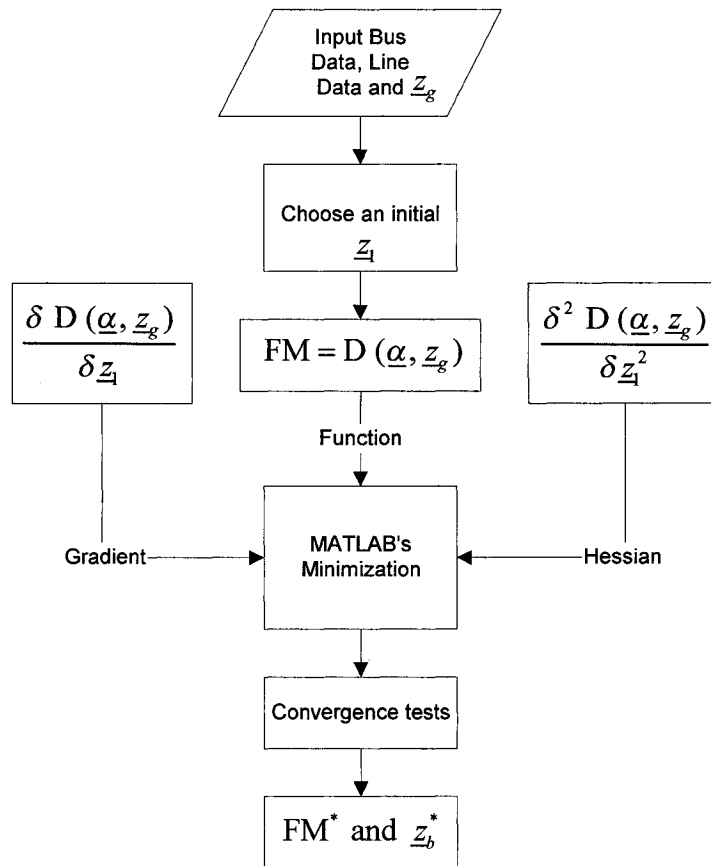


**Figure 2-14:** Flowchart of the optimization program

This program uses MATLAB's optimization function  $fmin(F(x), x_0, F'(x), F''(x))$  which optimizes a given function  $F(x)$  when provided with an initial guess  $x_0$  together with the Gradient  $F'(x)$  and Hessian  $F''(x)$  of the function. The program starts by collecting the bus and line data information of the network. An initial search direction  $\underline{z}$  is selected and the function to be optimized, namely the FM is formed as described in the previous program from,

$$\begin{aligned} \text{FM} &= \frac{\underline{\alpha}^T \underline{z}_g}{\|\underline{\alpha}\| \|\underline{z}_g\|} \\ &= D(\underline{\alpha}, \underline{z}_g) \end{aligned} \tag{2.92}$$

The MATLAB optimization is more robust when the first derivative of the optimization function is also provided as detailed in Appendix A.

### Chapter 3 : Study Cases of Load Flow Infeasibility

As was discussed in the previous chapter, the load flow feasibility region  $R_z$  is characterized by the structure of the power network, which involves the nature of the bus types and the bus admittance matrix,  $\bar{Y}$ . A network operating point which consists of the injection vectors  $\underline{P}$ ,  $\underline{Q}$  and  $\underline{V}^2$  for the load and voltage controlled buses is a feasible injection when it lies within the region  $R_z$ .

Load flow infeasibility studies examines events that make a given network injection  $\underline{z}_g$  to move close to the boundary of or outside  $R_z$ . This can occur via two different mechanisms. In the first, a change in the size and/or shape of the feasibility region places the feasible injection  $\underline{z}_g$  outside the boundary of  $R_z$ . Figure 3-1 shows a contingency resulting in such infeasibility. What events lead to this type of mechanism are discussed in section 3.1.

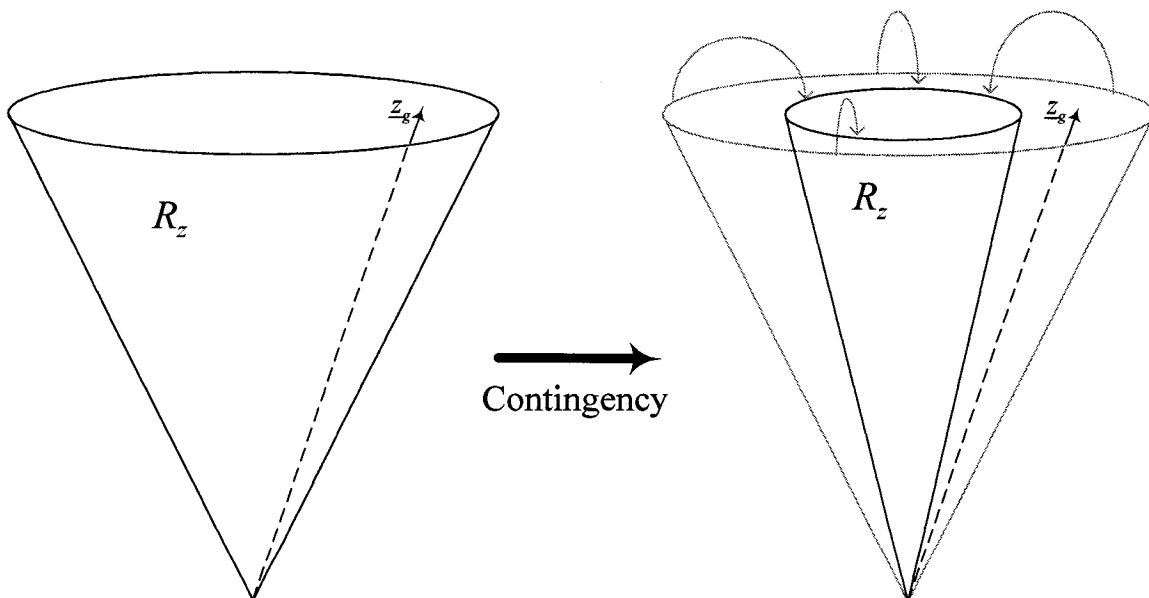


**Figure 3-1: Feasibility boundary movement**



In the second mechanism shown in Figure 3-2, the feasibility region  $R_z$  stays unchanged but the injection vector  $\underline{z}_g$  moves outside  $R_z$ . Depending on the nature of the event, this repositioning of  $\underline{z}_g$  may occur gradually or suddenly as detailed in section 3.2.

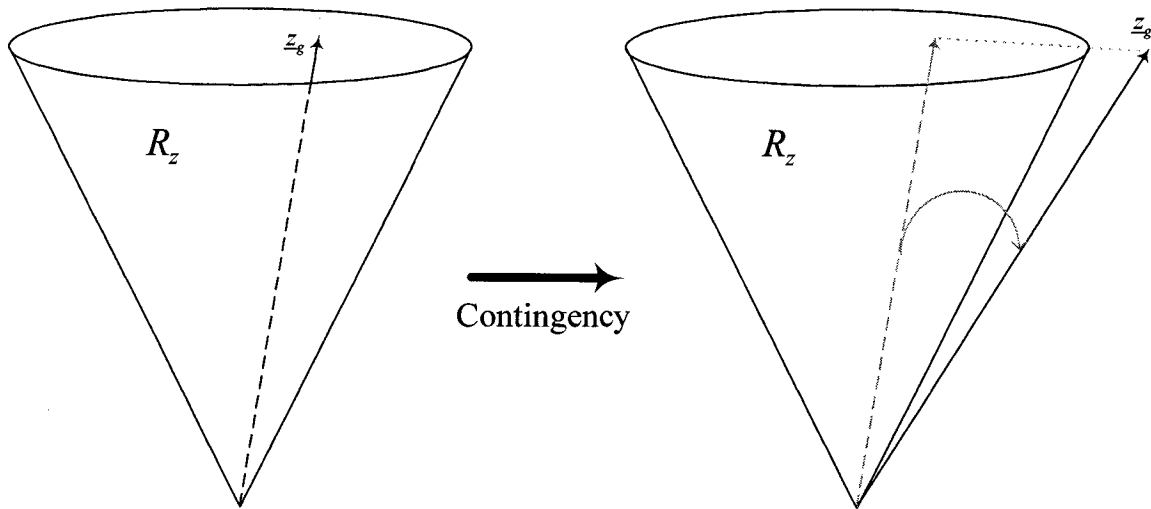


**Figure 3-2: Injection vector movement**

### 3.1 Feasibility boundary movement

The boundary of the feasibility region is described by the network structure, namely by the branches connecting the power network buses and by the presence or absence of voltage support capability at the buses. Therefore, in order for the load flow feasibility boundary to change or move, there needs to be a change in either of these aspects. A change in bus voltage support capability translates into a change in bus type. On the other hand, changes in branch connectivity are those involving loss of one or more transmission lines.

#### 3.1.1 Bus type change

When voltage control at a generator bus is lost, this results in changing a *PV* into a *PQ* bus. Therefore, studying bus type changes is useful in certain contingency cases, such as the loss of a generator or the saturation of the VAR supply capability at a bus.

These cases are better explained through examples. Consider a 5-bus network as shown in Figure 3-3. The branch information is provided in Appendix B.

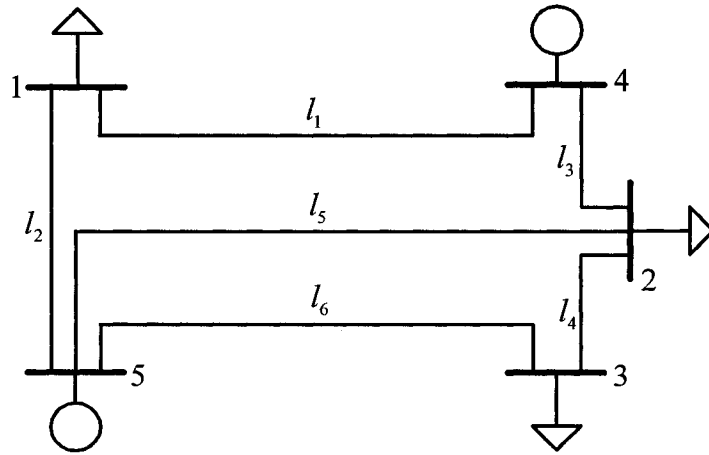


**Figure 3-3: 5-Bus network #1**

This 5-bus network consists of 3  $PQ$  (1, 2 and 3) and 1  $PV$  (4) bus and one slack (5). To look at the effect of a bus type change on feasibility consider the following injection vector.

$$\underline{z}_{g1} = [P_1, P_2, P_3, P_4, Q_1, Q_2, Q_3, V_4^2, V_5^2]^T$$

where,

$$\underline{z}_{g1} = [-0.6, -0.6, -0.4, 1.0, -0.2, -0.3, -0.1, 1.0, 1.0]^T \text{ (p.u.)}$$

The unspecified bus injection and voltage components for this given  $\underline{z}_g$  are obtained by solving the corresponding load flow and are provided in Table 3-1.

**Table 3-1: Load flow for 5-bus network #1**

Bus	Type	Injection		Voltage	
		$P$ (p.u.)	$Q$ (p.u.)	$V$ (p.u.)	$\delta$ (Degrees)
1	$PQ$	-0.6	-0.2	0.962	-2.018
2	$PQ$	-0.6	-0.3	0.920	-4.001
3	$PQ$	-0.4	-0.1	0.892	-8.408
4	$PV$	1.0	0.388	1.0	2.522
5	Swing	0.655	0.433	1.0	0

Let us now convert bus 4 from a  $PV$  into a  $PQ$  bus with the values of  $P_4$  and  $Q_4$  taken from Table 3-1. The new injection  $\underline{z}_{g2}$  is

$$\underline{z}_{g2} = [P_1, P_2, P_3, P_4, Q_1, Q_2, Q_3, Q_4, V_5^2]^T$$

where,

$$\underline{z}_{g2} = [-0.6, -0.6, -0.4, 1.0, -0.2, -0.3, -0.1, 0.388, 1.0]^T \text{ (p.u.)}$$

As defined in Equation (2.90), the FM values for these two different injections are shown in Table 3-2.

**Table 3-2: Feasibility margins for a change in bus type**

Injection	Feasibility margin
$\underline{z}_{g1}$	0.215
$\underline{z}_{g2}$	0.184

The change in the FM shows that although the network and load flow are the same, the new bus type structure changes the feasibility region and results in a lower FM of 0.184 versus 0.215. This is reasonable since the new network has less voltage control.

### 3.1.2 Change in network structure

The best example of a change in network structure is the loss of some transmission lines, which results in a change in the network's admittance matrix  $\bar{Y}$ , which then redistributes the current flows throughout the remaining network. This change in network structure also alters the shape of the feasibility region and changes the FM. The loss of lines can influence load flow feasibility differently; in a very severe case loss of several lines can result in infeasibility, i.e. a negative FM.

Consider now the 14-bus network of Figure 3-4. The branch data of the network is provided in Appendix B.

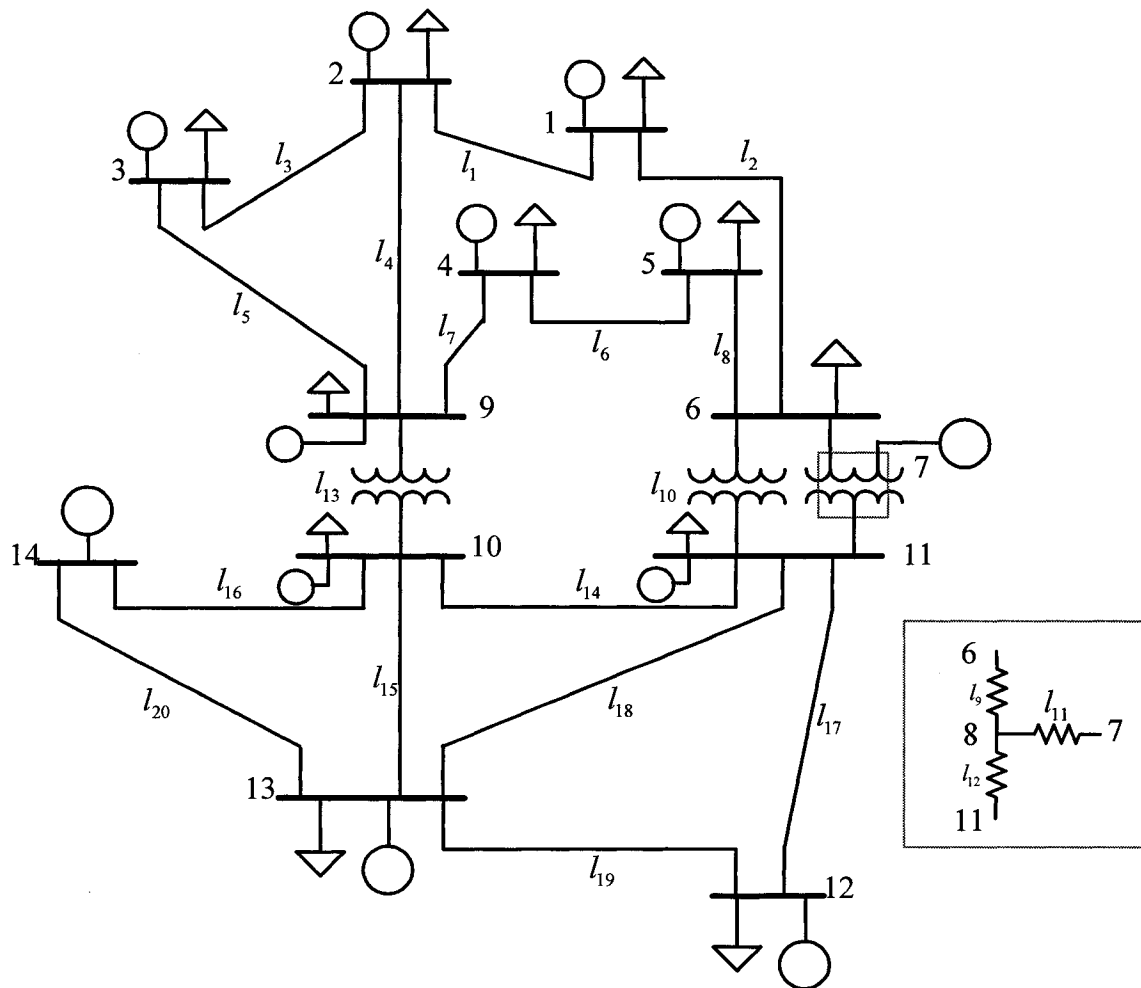


Figure 3-4: 14-bus Network

Let us consider the following given feasible injection,

**Table 3-3: Bus injections for 14-bus network**

Bus	Type	Injection		
		$P$ ( <i>p.u.</i> )	$Q$ ( <i>p.u.</i> )	$V^2$ ( <i>p.u.</i> )
1	<i>PQ</i>	0.154	-0.069	
2	<i>PQ</i>	0.627	-0.184	
3	<i>PQ</i>	0.149	-0.054	
4	<i>PQ</i>	0.219	-0.098	
5	<i>PQ</i>	0.052	-0.017	
6	<i>PQ</i>	0.016	0.102	
7	<i>PQ</i>	-0.248	0.005	
8	<i>PQ</i>	-0.033	0.003	
9	<i>PQ</i>	-0.674	0.374	
10	<i>PQ</i>	0.440	-0.182	
11	<i>PQ</i>	-0.259	-0.025	
12	<i>PQ</i>	-0.200	-0.032	
13	<i>PV</i>	-0.132		1
14	Swing			1

The lines are removed one by one (except line 11, since this line is connected directly to a generator) and the FM is calculated. The results are gathered in the following Table 3-4.

**Table 3-4: Line removal results**

Line removed	Feasibility margin
<i>Base case</i>	0.164
1	0.151
2	0.107
3	0.164
4	0.100
5	0.142
6	0.151
7	0.159
8	0.127
9	0.133
10	0.151
12	0.130
13	0.077
14	0.166
15	0.147
16	0.158
17	0.159
18	0.147
19	0.158
20	0.165

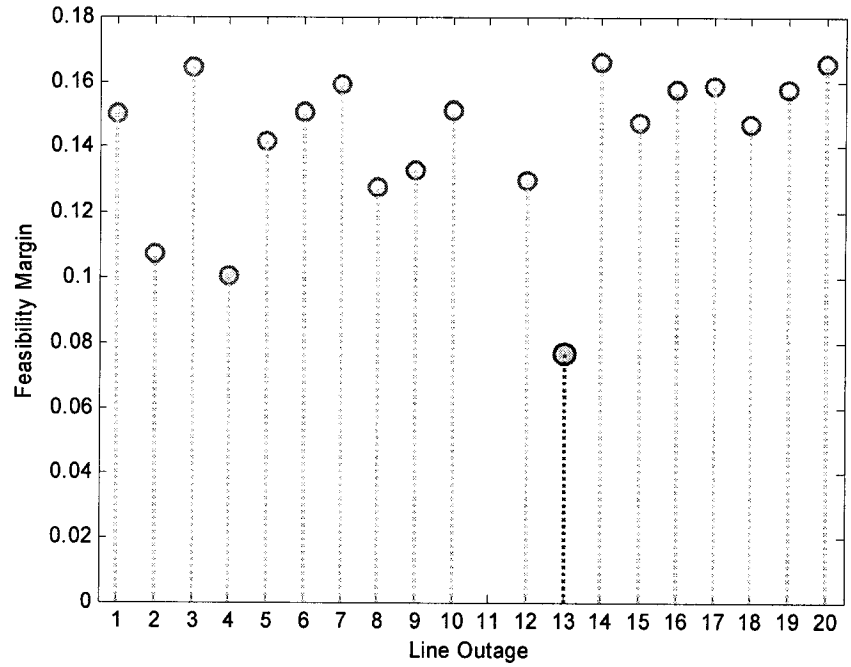


**Figure 3-5: Feasibility margin for different line removals**

It can be seen from Figure 3-5 that line 13 has the biggest effect on the FM. This is reasonable from the position of line 13 in the network as an important connection between its upper mostly generating sub-network and the lower part which is primarily consuming.

In the next step, let us start with a network without line 13 and observe the effect of further line losses. These results are shown in Table 3-5.

**Table 3-5: Line removal results with line 13 already out**

Line removed	Feasibility margin
<i>Base Case</i>	0.077
1	0.052
2	0.030
3	0.076
4	0.039
5	0.064
6	0.040
7	0.029
8	0.033
9	0.036
10	0.059
12	0.036
14	0.140
15	0.073
16	0.110
17	0.074
18	0.069
19	0.074
20	0.077

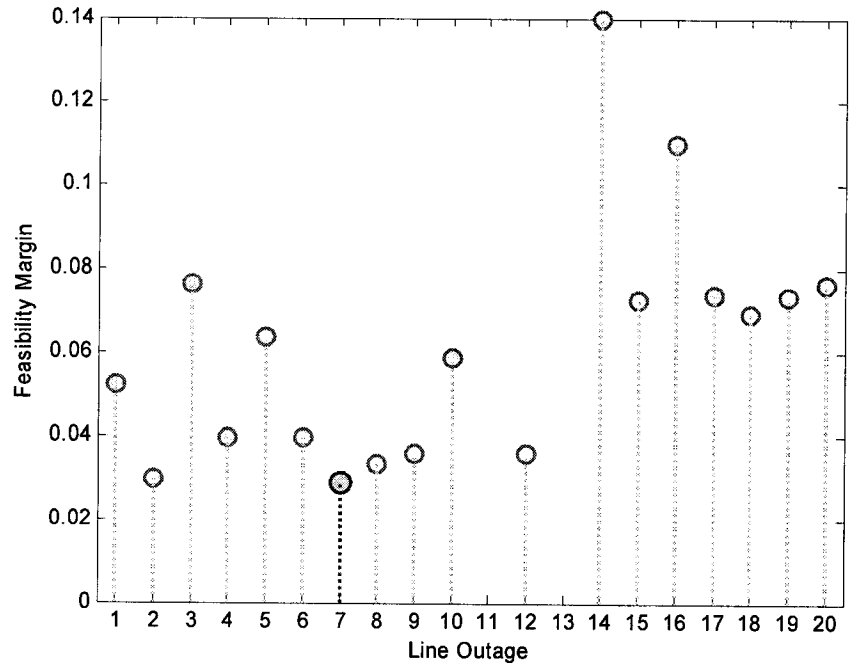


**Figure 3-6: Feasibility margin for different line removals with line 13 already out**

Hence the loss of line 7 yields the most severe effect. This process can be repeated again, this time with lines 7 and 13 out. The results are shown in Table 3-7. It is observed that the further loss of lines 1, 2, 4 and 6 result in infeasibility. Furthermore, the removal of

line 4 results in the lowest FM and hence has the worst effect. These observations are shown in Figure 3-7.

**Table 3-6:** Line removal results with lines 13 and 7 already out

Line removed	Feasibility margin
<i>Base Case</i>	0.029
1	-0.048
2	-0.047
3	0.027
4	-0.063
5	0.013
6	-0.049
8	0.201
9	0.013
10	0.023
12	0.013
14	0.131
15	0.028
16	0.158
17	0.028
18	0.026
19	0.028
20	0.029

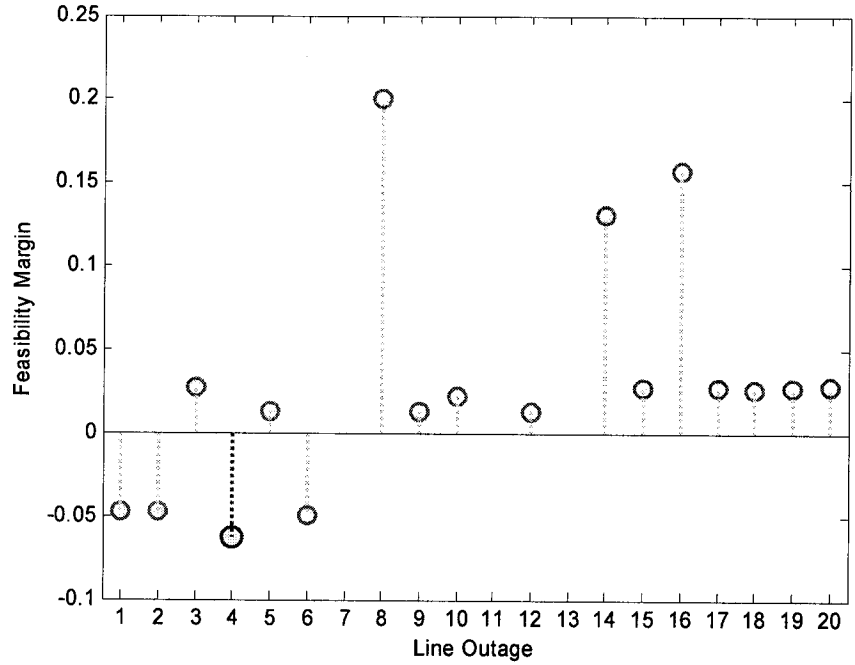


**Figure 3-7:** Feasibility margin for different line removals with lines 13 and 7 already out

To complete the test, let us consider a different injection vector,  $\underline{z}_g$ , one that loads the network more heavily, 2.39 p.u. compared to 1.546 p.u., as listed in Table 3-7.



**Table 3-7: New bus injections**

Bus	Type	Injection		
		$P$ (p.u.)	$Q$ (p.u.)	$V^2$ (p.u.)
1	$PQ$	-0.15	-0.05	
2	$PQ$	-0.14	-0.06	
3	$PQ$	-0.06	-0.02	
4	$PQ$	-0.04	-0.02	
5	$PQ$	-0.09	-0.06	
6	$PQ$	-0.3	-0.17	
7	$PQ$	0	0	
8	$PQ$	0	0	
9	$PQ$	-0.11	-0.08	
10	$PQ$	-0.08	-0.02	
11	$PQ$	-0.48	0.039	
12	$PQ$	-0.94	-0.19	
13	$PV$	0.18		1
14	Swing			1

We repeat the same procedure of line removal (except line 11), and summarize the effects in Table 3-8.

**Table 3-8: Line removal results**

Line removed	Feasibility margin
<i>Base Case</i>	0.093
1	0.090
2	0.042
3	0.093
4	0.056
5	0.079
6	0.091
7	0.090
8	0.059
9	0.030
10	0.065
12	0.028
13	-0.022
14	0.087
15	0.059
16	0.113
17	0.088
18	0.052
19	0.007
20	0.003

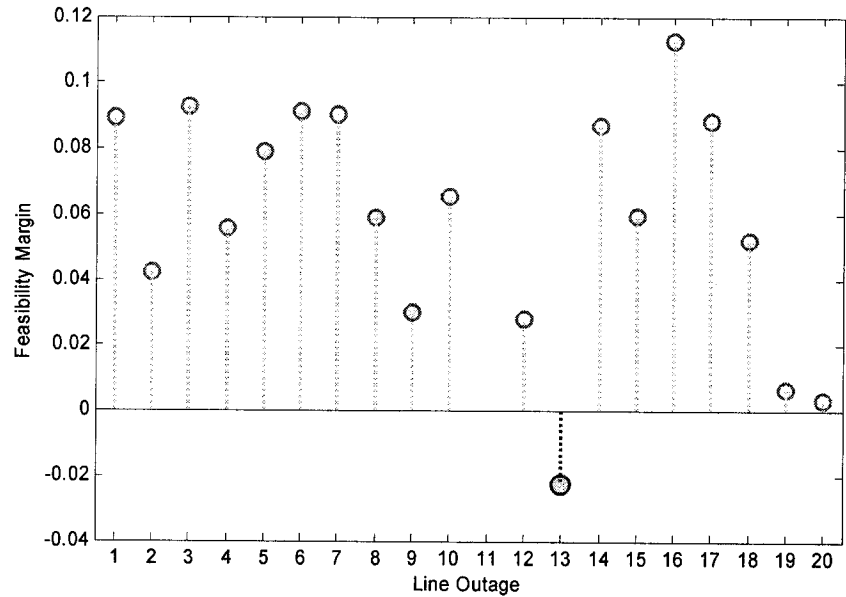


**Figure 3-8: Feasibility margin for different line removals**

As can be observed in Figure 3-8, line 13 again plays a big role on feasibility. Only this time, since the network is more heavily loaded the removal of line 13 results in infeasibility.

A possible future study would be to find a combination of a given number of lines whose outage would result in the most negative possible FM in a way that does not involve full enumeration as done above, but which would involve nonlinear mixed integer programming.

### 3.2 Movement of the nodal injection vector

Here, we examine the effect on feasibility of the nodal injection movement due to a change in the  $\underline{P}$ ,  $\underline{Q}$  or  $\underline{V}^2$  values, either gradually or suddenly.

#### 3.2.1 Gradual change

An example of a gradual change in the injection is that due to an increase in VAR demand at a  $PQ$  bus.

Let us start with the 3-bus network shown in Figure 3-9 as an example.

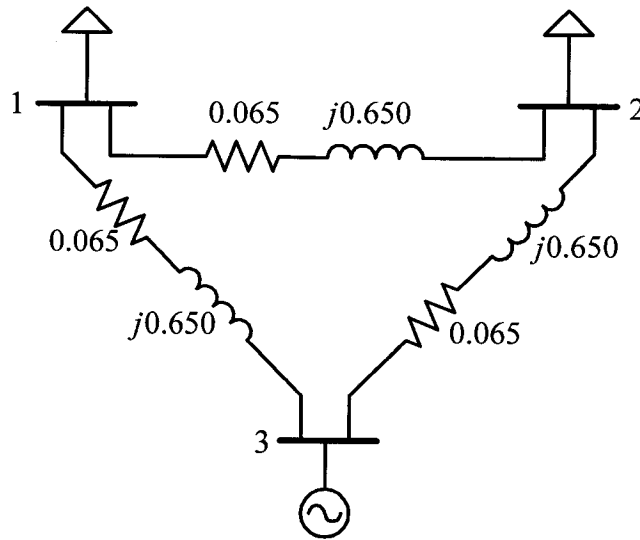


Figure 3-9: 3-bus network

The given injection and nodal voltage values are listed in Table 3-9.

**Table 3-9: Load flow**

Bus	Type	Injection		Voltage	
		$P$ (p.u.)	$Q$ (p.u.)	$V$ (p.u.)	$\delta$ (Degrees)
1	PQ	0	-0.1	0.927	0.412
2	PQ	0	-0.2	0.909	0.525
3	Swing	0.003	0.328	1.0	0

Consider the effect of a gradual change in the injection  $Q$  at bus 2. The resulting change in FM is listed in Table 3-10 and plotted in Figure 3-10.

**Table 3-10: Change in feasibility margin due to the change in  $Q$** 

$Q_2$	-0.2	-0.3	-0.4	-0.5	-0.6	-0.7	-0.8
FM	0.379	0.300	0.221	0.145	0.074	0.008	-0.052

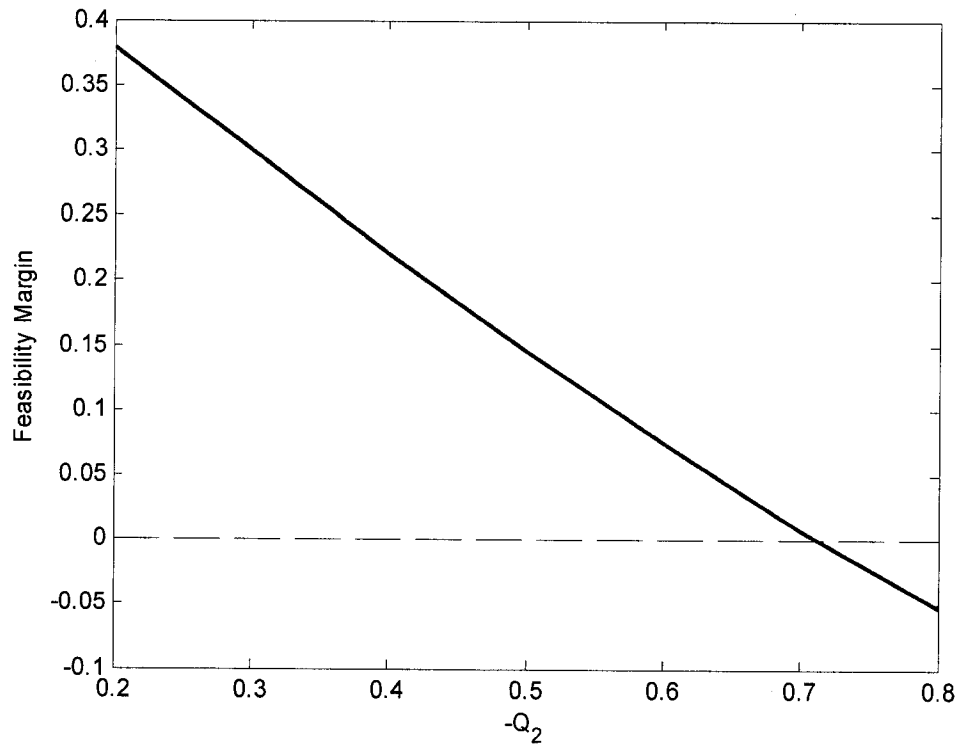


**Figure 3-10:** Graph of the change in feasibility margin as  $Q_2$  decreases

It can be seen that an increase in reactive demand at bus 2 results in a lower FM and eventually in infeasibility. This is expected, since VAR support is very important to voltage support. Figure 3-11 shows the value of the nodal voltages as  $Q_2$  is decreased.

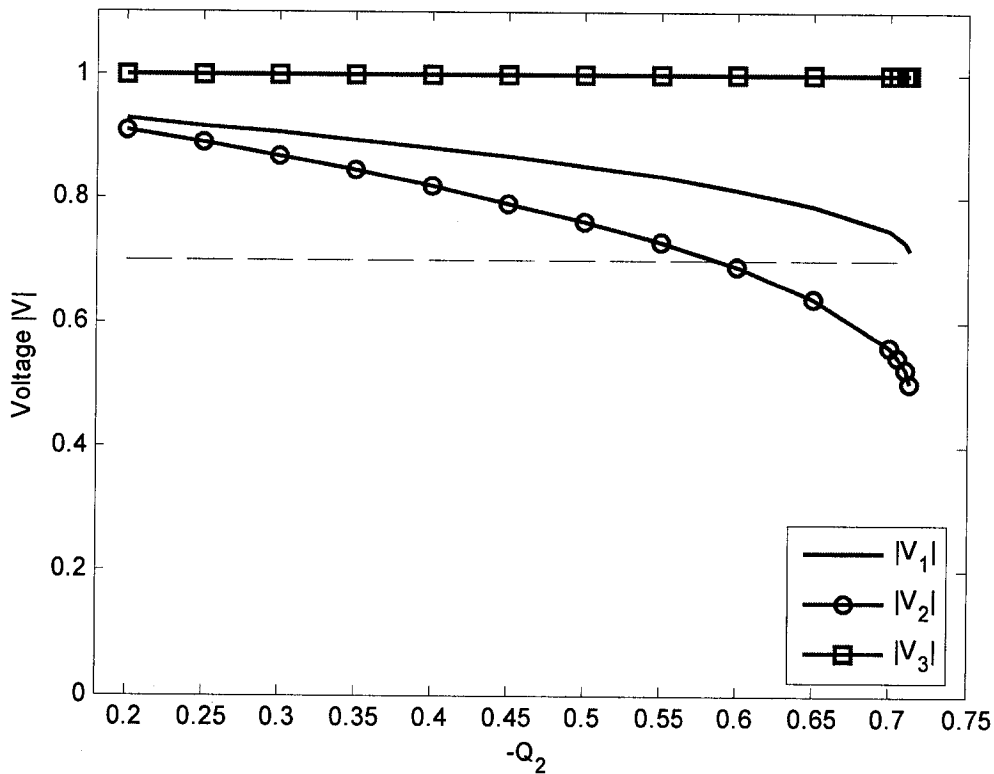


**Figure 3-11:** Change in the magnitude of the nodal voltages

It is observed that the voltage at bus 2, where the loss of  $Q$  support happens, drops more rapidly than the ones of the other two buses. When  $Q_2 = -0.6 \text{ p.u.}$ , the value of the voltage at bus 2 is lower than  $0.7 \text{ p.u.}$  which is an unacceptably low voltage even though the FM is still bigger than zero.

Note that the voltage curves in Figure 3-11 go all the way to the boundary of  $R_c$  at  $Q_2 = -0.713 \text{ p.u.}$ . This is not possible with methods based on load flow calculations.

It is also useful to look at the effect of this increase in the reactive demand at bus 2 on the angle of the voltages and the total transmission loss of the network. Figure 3-12 shows the change in angle difference for each line as  $Q_2$  decreases and Figure 3-13 shows the change in the total transmission loss of the network.

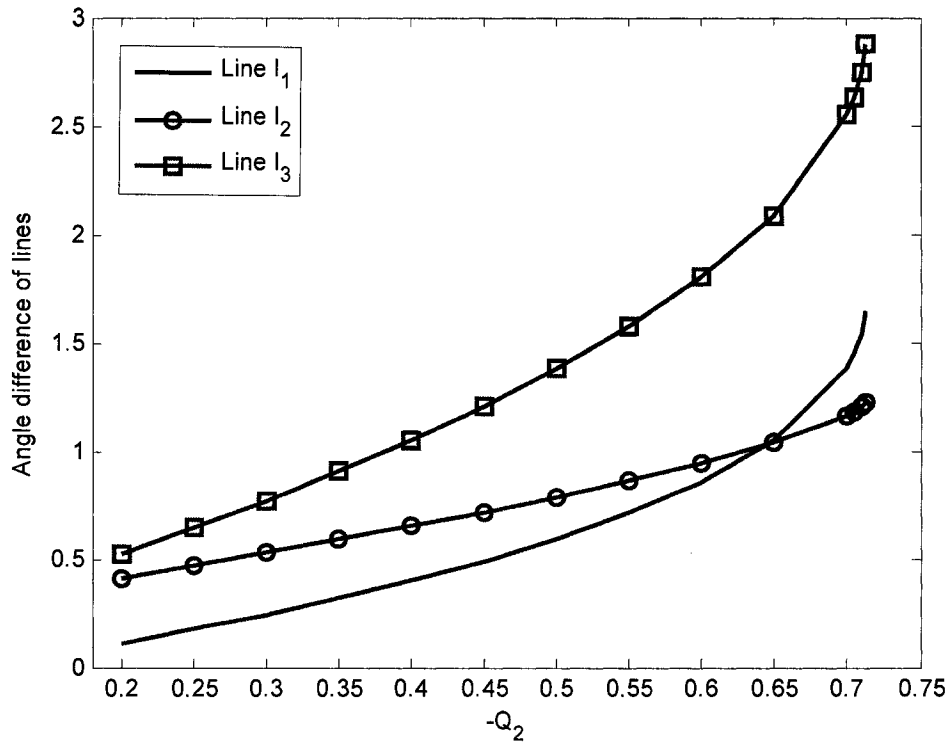


**Figure 3-12:** Change in the angle difference for each line

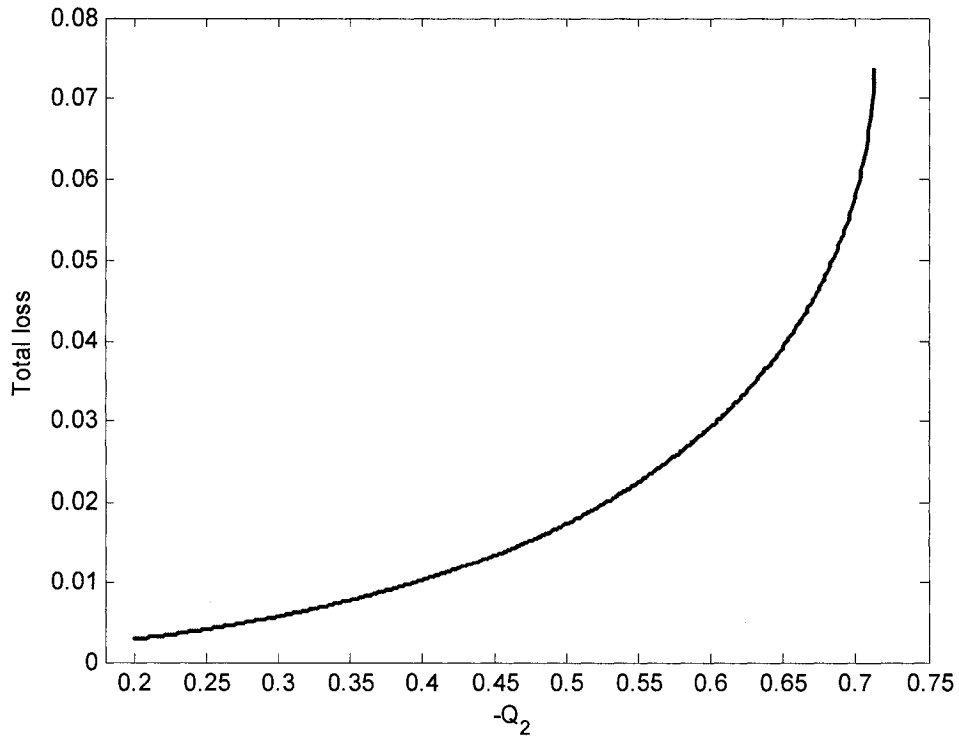


**Figure 3-13:** Change in the total transmission loss in the network

A decrease in  $Q_2$ , results in a bigger angle difference for the lines. This in turn increases the power flow in each line and therefore the transmission loss.

In addition when the network gets closer to infeasibility, the Jacobian matrix comes closer to singularity. This can be shown by observing the eigenvalues of the Jacobian matrix in Figure 3-14.

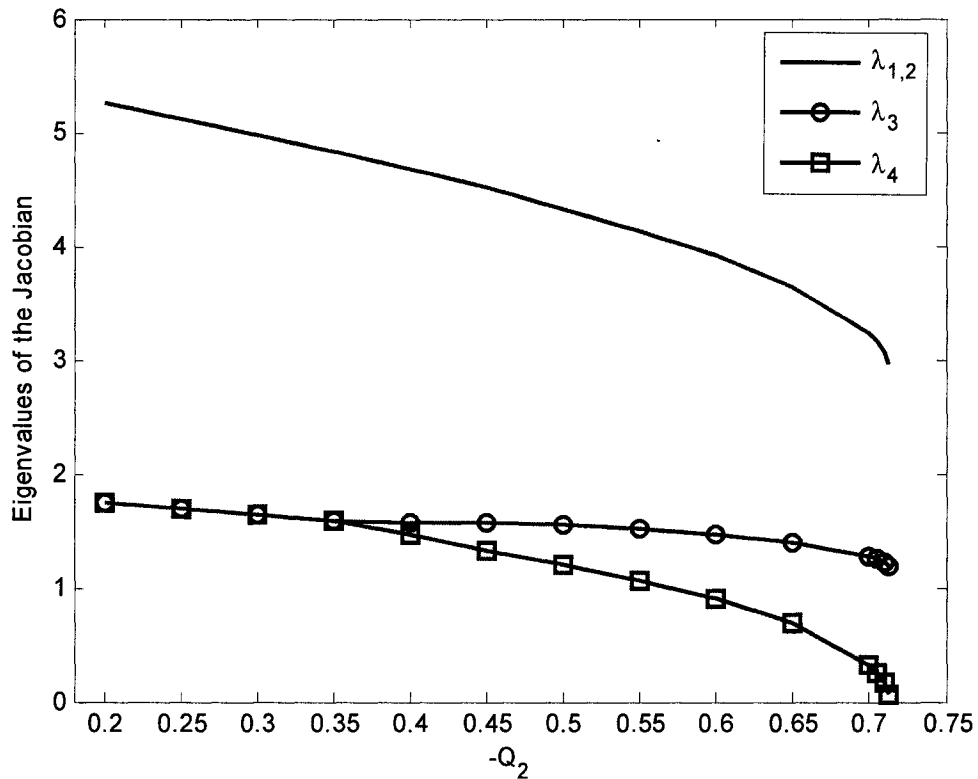


**Figure 3-14:** Change in the eigenvalues of the Jacobian

All eigenvalues including the complete conjugates ( $\lambda_1$  and  $\lambda_2$ ) decrease as  $Q_2$  decreases and the network is brought closer to infeasibility.  $\lambda_4$  however, is the eigenvalue the most effected. As this eigenvalue becomes zero the Jacobian becomes singular and the system infeasible.

Let us now consider a 5-bus network shown in Figures 3.15. Its line data is provided in Appendix B.



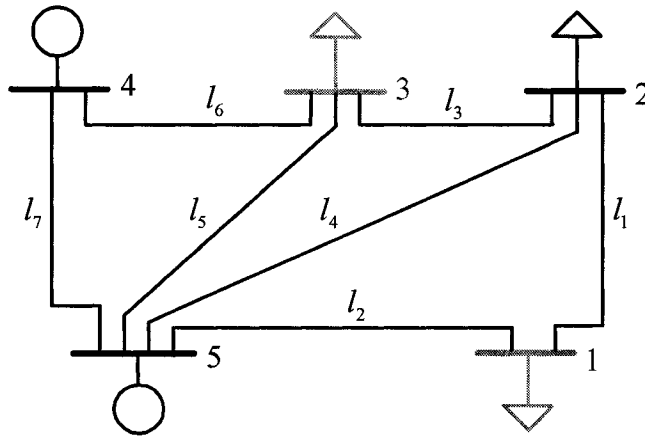


**Figure 3-15: 5-Bus network #2**

The injections and nodal voltages are as follows.

**Table 3-11: Load flow for 5-bus network #2**

Bus	Type	Injection		Voltage	
		$P$ (p.u.)	$Q$ (p.u.)	$V$ (p.u.)	$\delta$ (Degrees)
1	$PQ$	-0.489	0.2	1.004	-3.663
2	$PQ$	-0.566	0.176	1.001	-3.281
3	$PQ$	-0.244	0.1	1.001	-2.691
4	$PV$	0.830	-0.281	1.0	1.687
5	Swing	0.502	0.211	1.0	0

As shown in the previous 3-bus example, a decrease in the imaginary power  $Q$  at a  $PQ$  bus will result in the loss of voltage support and moves the given injection towards infeasibility. However, it is useful to know which  $PQ$  bus has the most important  $Q$  support role in the network, i.e. a decrease of  $Q$  at which bus would affect the FM most significantly. This is realized by looking at the  $\underline{\alpha}$  vector calculated for the given injection

$$\underline{z}_g \cdot$$

**Table 3-12:**  $\underline{\alpha}$  values for the given injection  $\underline{z}_g$

$\alpha_{P1}$	$\alpha_{P2}$	$\alpha_{P3}$	$\alpha_{P4}$	$\alpha_{Q1}$	$\alpha_{Q2}$	$\alpha_{Q3}$	$\alpha_{V^2_1}$	$\alpha_{V^2_2}$
0.417	0.096	0.076	0.033	0.238	0.055	0.040	-0.004	2.566

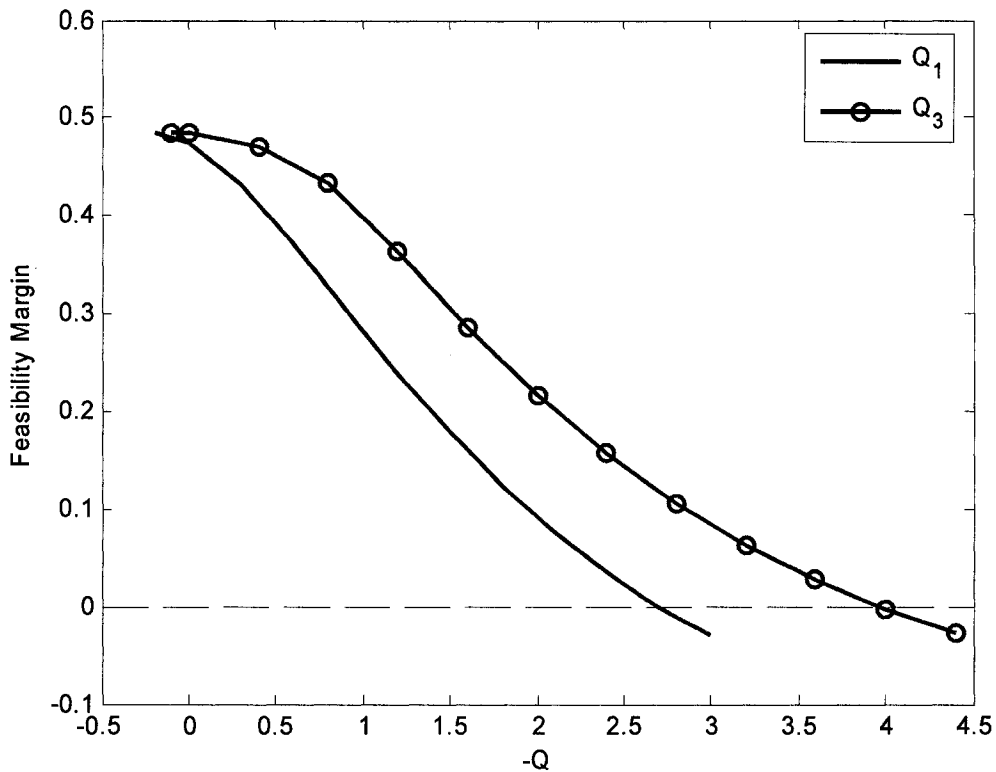
As it was discussed in section 2.3.2, the  $\underline{\alpha}$  vector is a measure of sensitivity of the FM with respect to changes in the given injection,  $\underline{z}_g$ . Thus the bus with the higher value of  $\alpha_Q$  would have the biggest impact on the *F.M.*

Table 3-13 shows the change in the value of the FM as  $Q_1$  and  $Q_3$  decrease.

**Table 3-13:** Feasibility margin due to imaginary power decrease at bus 1 and 3

$Q_1$	<i>F.M.</i>	$Q_3$	<i>F.M.</i>
0.2	0.485	0.1	0.485
0.0	0.473	0.0	0.485
-0.3	0.432	-0.4	0.469
-0.6	0.372	-0.8	0.433
-0.9	0.305	-1.2	0.363
-1.2	0.239	-1.6	0.287
-1.5	0.179	-2.0	0.217
-1.8	0.124	-2.4	0.157
-2.1	0.077	-2.8	0.106
-2.4	0.036	-3.2	0.064
-2.7	0.0	-3.6	0.028
-3.0	-0.030	-4.0	-0.002
		-4.4	-0.028

The results in Table 3-13 show that the FM is more sensitive to the changes in the value of  $Q_1$  than  $Q_3$ . This agrees with the values of  $\alpha_{Q1}$  and  $\alpha_{Q2}$  and is better illustrated in Figure 3-16.



**Figure 3-16:** Feasibility margin due to imaginary power decrease at bus 1 and 3

### 3.2.2 Sudden change

Loss of a generator is one of the contingencies which can affect a power network severely. This is due to a sudden loss in both  $P$  and  $Q$  at the bus connected to the generator. It is important to note that a generator bus is a  $PV$  bus where the values of  $P$  and  $V^2$  can be set, however a loss in generator requires the values of  $P$  and  $Q$  in the bus to both be set to zero. Therefore in simulation, generator loss translates into a type conversion from  $PV$  to  $PQ$  in that specific bus.

As an example, let us consider the 5-bus example in Figure 3-17.

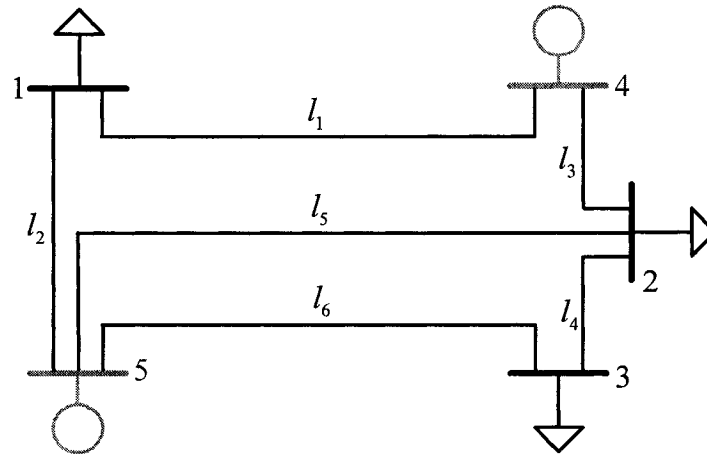


**Figure 3-17: 5-bus network #1**

The injection and voltage values are listed in Table 3-14.

**Table 3-14: Original load flow for 5-bus network #1**

Bus	Type	Injection		Voltage	
		$P$ (p.u.)	$Q$ (p.u.)	$V$ (p.u.)	$\delta$ (Degrees)
1	$PQ$	-0.6	-0.2	0.962	-2.018
2	$PQ$	-0.6	-0.3	0.920	-4.001
3	$PQ$	-0.4	-0.1	0.892	-8.408
4	$PV$	1.0	0.388	1.0	2.522
5	Swing	0.655	0.433	1.0	0

First, we look at the effect of the loss of the generator at bus 4. As explained before, this is done by changing bus 4 from a  $PV$  into a  $PQ$  and then setting the  $P$  and  $Q$  values to zero. The new injection and nodal values are as following.

**Table 3-15:** Load flow for 5-bus network #1 after loss of the generator at bus 4

Bus	Type	Injection		Voltage	
		$P$ (p.u.)	$Q$ (p.u.)	$V$ (p.u.)	$\delta$ (Degrees)
1	PQ	-0.6	-0.2	0.877	-8.794
2	PQ	-0.6	-0.3	0.816	-12.651
3	PQ	-0.4	-0.1	0.819	-14.106
4	PQ	0	0	0.846	-10.650
5	Swing	1.722	1.087	1.0	0

The same thing can be done for the loss of the generator at bus 5. In this case, the swing bus is bus 4. These results are as follows.

**Table 3-16:** Load flow for 5-bus network #1 after loss of the generator at bus 5

Bus	Type	Injection		Voltage	
		$P$ (p.u.)	$Q$ (p.u.)	$V$ (p.u.)	$\delta$ (Degrees)
1	PQ	-0.6	-0.2	0.877	-8.938
2	PQ	-0.6	-0.3	0.841	-10.527
3	PQ	-0.4	-0.1	0.773	-18.632
4	Swing	1.725	1.1	1.0	0
5	PQ	0	0	0.847	-10.972

The FMs of the networks corresponding to the loss of generator in bus 4 or 5 are summarized in Table 3-17.

**Table 3-17:** Change in feasibility margin for the loss of each generator

Generator loss	None	4	5
Feasibility margin	0.2154	0.1559	0.0618

It is observed that a generation outage causes a drop in FM. This drop is bigger in case of the generator in bus 5. This is because bus 5 is connected to more buses in the network than bus 4. Therefore, in an event of outage in bus 4, the generator at bus 5 can support most of the network directly. In contrast, if the outage is at bus 5, the generator at bus 4 does not have as good access to the rest of the network. However, in both cases the contingency is not severe enough to bring the system to infeasibility.

Now let us consider the same network as in Figure 3-17 but more heavily loaded. The total load is increased from 1.6 *p.u.* to 2 *p.u.*. The injection and the nodal voltage values are listed in the Table 3-18.

**Table 3-18:** Original load flow for 5-bus network #1 (Higher Load)

Bus	Type	Injection		Voltage	
		<i>P</i> ( <i>p.u.</i> )	<i>Q</i> ( <i>p.u.</i> )	<i>V</i> ( <i>p.u.</i> )	$\delta$ (Degrees)
1	<i>PQ</i>	-0.75	-0.2	0.957	-4.412
2	<i>PQ</i>	-0.75	-0.3	0.908	-7.394
3	<i>PQ</i>	-0.5	-0.1	0.872	-12.241
4	<i>PV</i>	1.0	0.473	1.0	-0.435
5	Swing	1.082	0.456	1.0	0

If the generator at bus 4 is out, the new injection values are:

**Table 3-19:** Load flow for 5-bus network #1 (Higher Load) after loss of the generator at bus 4

Bus	Type	Injection		Voltage	
		$P$ (p.u.)	$Q$ (p.u.)	$V$ (p.u.)	$\delta$ (Degrees)
1	PQ	-0.75	-0.2	0.848	-11.662
2	PQ	-0.75	-0.3	0.773	-17.169
3	PQ	-0.5	-0.1	0.771	-19.194
4	PQ	0	0	0.810	-14.287
5	Swing	2.201	1.403	1.0	0

And in the case where, the generator at bus 5 is out, the injection values are:

**Table 3-20:** Load flow for 5-bus network #1 (Higher Load) after loss of the generator at bus 5

Bus	Type	Injection		Voltage	
		$P$ (p.u.)	$Q$ (p.u.)	$V$ (p.u.)	$\delta$ (Degrees)
1	PQ	-0.75	-0.2	0.845	-11.893
2	PQ	-0.75	-0.3	0.798	-14.217
3	PQ	-0.5	-0.1	0.7073	-26.065
4	Swing	2.212	1.448	1.0	0
5	PQ	0	0	0.804	-14.768

The FMs, corresponding to these new situations are listed in Table 3-21.

**Table 3-21:** Change in feasibility margin for the loss of each generator

Generator loss	None	4	5
Feasibility margin	0.174	0.088	-0.011

As before, the effect of the outage in bus 5 is more severe than that in bus 4. However, due to the heavy load in the network, an outage in bus 5 is effective enough to cause infeasibility.



## Chapter 4: Conclusions

### 4.1 Summary

We have studied the feasibility of power flows through the notion of the power flow feasibility region. To characterize such a region, we have made use of the supporting hyperplane method and the notion of feasibility region on a plane. We showed in detail how supporting hyperplanes are calculated and used to find the closest boundary injection to a specified vector of load flow injections.

The supporting hyperplane method proved to be much more powerful than using the conventional load flow in finding points on the boundary of the feasibility region. The load flow equations were difficult to solve when the specified injections were in the proximity of the feasibility boundary, as the load flow Jacobian became ill-conditioned. In contrast, the supporting hyperplane method was able to find the closest injection on the boundary of feasibility to the injection through systematic steps that did not give rise to the numerical difficulties associated with the near singularity of the load flow Jacobian matrix. Furthermore, the hyperplane method provided the feasibility margin (FM), which measures the degree of the feasibility of the specified injections.

The method of supporting hyperplanes presented an effective way of finding the failure path with the highest impact on the feasibility of an injection. Different mechanisms were used to characterize this path; some were based on changing the feasibility region whereas others involved altering the injection itself.

Changes to the feasibility region were achieved by bus type change and line outages. It was shown that changing the type of a bus affects the FM. Converting a  $PV$  bus to a  $PQ$  bus reduced the FM as it resulted in the loss of voltage support at the bus. Line outages also decreased the FM. Thus, it was shown that the severity of line outages on the FM depends on the location of the removed lines as well as on the loading of the network. The loss of a combination of lines, which were part of the main power flow path between

generation sites and demand points, resulted in infeasibility. For higher loading levels, fewer such outages were however required to drive an injection to infeasibility

Other mechanisms deforming the feasibility region included gradual and sudden changes in the given injection. Thus, a gradual increase in VAR demand at a bus was shown to reduce voltage support and drive the injection towards the boundary of feasibility and reduce the FM. Moreover, the  $\underline{\alpha}$  vector was shown to provide a measure of sensitivity, identifying the bus at which a demand increase makes the network more vulnerable to infeasibility. Additionally, the effect of generation loss on the FM was studied. For a heavily loaded system, it was shown that, in most cases, a severe case of this type can readily be found leading to immediate infeasibility.

These results further supported the claim that the hyperplane method is a powerful tool for analyzing the impact of extreme contingencies on the feasibility of power flows.

#### **4.2 Suggestions for Further Research**

The feasibility margin as an indicator of the vulnerability of power networks to extreme contingencies could be examined for large networks over extended periods of time. In choosing alternatives for expanding a transmission network, the level of increase in the network FM could be an additional selection criterion. However, the prerequisite for enforcing such a criterion is the ability to establish an acceptable minimum FM of a given power system. Developing a methodology to determine this minimum would be an interesting area of research.

## Bibliography

- [1] P. Kundur, *Power Systems Stability and Control*, McGraw-Hill, New York, 1994.
- [2] H.D. Chiang, I. Dobson, R.J. Thomas, J.S. Thorp, L. Fekih-Ahmed, "On Voltage Collapse in Electric Power Systems," *IEEE Transactions on Power Systems*, Vol. 5, Issue 2, May 1990.
- [3] I.O. Elgerd, *An Introduction to Electric Energy Systems*. Second Edition, McGraw-Hill Book Company, New York, 1982.
- [4] G.W. Stagg and A.H. El-Abiad, *Computer Methods in Power System Analysis*, McGraw-Hill, New York, 1968.
- [5] J.S. Throp, S.A. Nagavi, "Load-flow Fractals draw Clues to Erratic Behavior," *IEEE Computer Applications in Power*, Vol. 10, Issue 1, pp. 59-62, Jan. 1997.
- [6] J. Jarjis, "Analysis and Characterization of Security Regions in Power Systems," ph.D. thesis, Dept. Comp. & Elec. Eng., McGill Univ., Montreal, Quebec, March 1980.
- [7] R.B.L. Guedes, L.F.C. Alberto, N.G. Bretas, "The electrical coupling effect on the behaviour of the load flow solutions for voltage collapse purposes," in *IEEE Power Engineering Society General Meeting*, Vol. 2, June 2004, pp. 1820-1825.
- [8] N. Yorino, S. Harada, C. Haozhong, "A method to approximate a closest loadability limit using multiple load flow solutions," *IEEE Transactions on Power Systems*, Vol. 12, Issue 1, pp. 424 - 429, Feb. 1997.
- [9] Z.C. Zeng, F.D. Galiana, B.T. Ooi, N. Yorino, "A simplified approach to estimate maximum loading conditions in the load flow problem," *IEEE Trans. on Power Systems*, Vol. 8, Issue 2, pp. 646 - 654, May 1993.
- [10] N. Yorino, S. Harada, H.Q. Li, A.Ohta, H. Sasaki, "A method of voltage stability evaluation for branch and generator outage contingencies," *IEEE Transactions on Power Systems*, Vol. 19, Issue 1, pp. 252 - 259, Feb. 2004.
- [11] F.D. Galiana, K. Lee, "Power Voltage Limitation imposed by the Network Structure of a Power System," *Proc. of the Power Industry and Computer Applications*, pp. 356-365, 1975.

- [12] F.D. Galiana, K. Lee, "On the steady State Stability of Power Systems," *Proc. Of the Power Industry and Computer Applications*, pp. 201-210, Toronto, May 1977.
- [13] J. Jarjis, F.D. Galiana, "Quantitative Analysis of Steady State Stability in Power networks," Paper F79 753-5, *IEEE Summer Power Meeting*, Vancouver, July 1979.
- [14] A.G. Expósito, *ANÁLISIS Y OPERACIÓN DE SISTEMAS DE ENERGÍA ELÉCTRICA*. First Edition, McGraw-Hill, 2002
- [15] F.D. Galiana, Z.C. Zeng, "Analysis of the load flow behavior near a Jacobian singularity," in 1991 *Power Industry Computer Application Conf. Proc.*, pp. 149-155.
- [16] F.D. Galiana, M. Banakar, "Realizability inequalities for security constrained load flow variables," *IEEE Trans. on Circuits and Systems*, Vol. 29, Issue 11, pp.767 - 772, Nov. 1982.

## Appendix A

### The Gradient

The function whose derivative we seek with respect to the search direction  $\underline{z}_1$  is,

$$D(\underline{\alpha}, \underline{z}_g) = \frac{\underline{\alpha}^T \underline{z}_g}{\|\underline{\alpha}\| \|\underline{z}_g\|} \quad (\text{A.1})$$

where,

$$\underline{\alpha} = \lambda_{\max} \underline{z}_0 - \underline{z}_1 \quad (\text{A.2})$$

or

$$\underline{\alpha} = \underline{z}_1 - \lambda_{\min} \underline{z}_0 \quad (\text{A.3})$$

Using the chain rule, the first order expansion of the function gives,

$$\delta D = \frac{1}{\|\underline{\alpha}\| \|\underline{z}_g\|} \delta(\underline{\alpha}^T \underline{z}_g) + \frac{\underline{\alpha}^T \underline{z}_g}{\|\underline{z}_g\|} \delta\left(\frac{1}{\|\underline{\alpha}\|}\right) \quad (\text{A.4})$$

But since,

$$\delta(\underline{\alpha}^T \underline{z}_g) = \delta(\underline{\alpha}^T) \underline{z}_g \quad (\text{A.5})$$

and,

$$\delta\left(\frac{1}{\|\underline{\alpha}\|}\right) = -\frac{\delta(\underline{\alpha}^T) \underline{\alpha}}{\underline{\alpha}^T \underline{\alpha} \|\underline{\alpha}\|} \quad (\text{A.6})$$

Substituting (A.5) and (A.6) into Equation (A.4), after some rearrangement, yields,

$$\frac{\delta D}{\delta \underline{\alpha}} = \frac{1}{\|\underline{\alpha}\|} \left[ \underline{I} - \frac{\underline{\alpha}^T \underline{z}_g}{\underline{\alpha}^T \underline{\alpha}} \right] \frac{\underline{z}_g}{\|\underline{z}_g\|} \quad (\text{A.7})$$

which is the gradient of the objective function (A.1) with respect to the vector  $\underline{\alpha}$ . However, since the optimization is searching over the direction vector  $\underline{z}_1$ , we must express the gradient with respect to  $\underline{z}_1$ . This can be done by expressing  $\delta \underline{\alpha}$  in (A.7) in terms of  $\delta \underline{z}_1$ . When the extreme eigenvalue is  $\lambda_{\max}$ , this can be done from,

$$\underline{\alpha} = \lambda \underline{z}_0 - \underline{z}_1 \quad (\text{A.8})$$

Differentiating (A.8) with respect to  $\underline{z}_1$  results in,

$$\delta \underline{\alpha} = \delta \lambda \underline{z}_0 - \delta \underline{z}_1 \quad (\text{A.9})$$

Upon pre-multiplying by  $\underline{z}_b^T$ , (A.9) becomes,

$$\underline{z}_b^T \delta \underline{\alpha} = \delta \lambda \underline{z}_b^T \underline{z}_0 - \underline{z}_b^T \delta \underline{z}_1 \quad (\text{A.10})$$

But since it has been shown in (2.88) that  $\underline{\alpha}^T \underline{z}_b = 0$ , we can also show that,

$$\underline{z}_b^T \delta \underline{\alpha} = 0 \quad (\text{A.11})$$

To prove (A.11), consider the relation (2.87),

$$\underline{J}(\underline{\alpha}) \underline{x}_b = \underline{0} \quad (\text{A.12})$$

For small deviations,

$$\underline{J}(\delta \underline{\alpha}) \underline{x}_b + \underline{J}(\underline{\alpha}) \delta \underline{x}_b = \underline{0} \quad (\text{A.13})$$

Pre-multiplying by  $\underline{x}_b^T$  gives,

$$\underline{x}_b^T \underline{J}(\delta \underline{\alpha}) \underline{x}_b + \underline{x}_b^T \underline{J}(\underline{\alpha}) \delta \underline{x}_b = \underline{0} \quad (\text{A.14})$$

However from (A.12), the second term of (A.14) is zero and it beomes,

$$\underline{x}_b^T \underline{J}(\delta \underline{\alpha}) \underline{x}_b = 0 \quad (\text{A.15})$$

using the identity in (2.86), Equation (A.15) becomes,

$$\underline{z}_b^T \delta \underline{\alpha} = 0 \quad (\text{A.16})$$

which is the desired result. Thus, incorporating this result into (A.10) gives,

$$\delta \lambda \underline{z}_b^T \underline{z}_0 - \underline{z}_b^T \delta \underline{z}_1 = 0 \quad (\text{A.17})$$

which implies that,

$$\delta \lambda = \frac{\underline{z}_b^T \delta \underline{z}_1}{\underline{z}_b^T \underline{z}_0} \quad (\text{A.18})$$

The expression for  $\delta \underline{\alpha}$  in terms of  $\delta \underline{z}_1$  can now be obtained by substituting (A.18) into (A.9)

$$\delta \underline{\alpha} = \left[ \frac{\underline{z}_0 \underline{z}_b^T}{\underline{z}_0^T \underline{z}_b^T} - \underline{I} \right] \delta \underline{z}_1 \quad (\text{A.19})$$

Using this expression for  $\delta \underline{\alpha}$ , the original gradient function (A.7) can be written with respect to  $\underline{z}_1$ ,

$$\frac{\delta D}{\delta \underline{z}_1} = \frac{1}{\|\underline{\alpha}\|} \left[ \frac{\underline{z}_0 \underline{z}_b^T}{\underline{z}_0^T \underline{z}_b} - I \right] \left[ I - \frac{\underline{\alpha} \underline{\alpha}^T}{\underline{\alpha}^T \underline{\alpha}} \right] \frac{\underline{z}_g}{\|\underline{z}_g\|} \quad (\text{A.20})$$

which can be written in the following form,

$$\frac{\delta D}{\delta \underline{z}_1} = \frac{1}{\|\underline{\alpha}\| \|\underline{z}_g\|} [T_1 \underline{z}_b + T_2 \underline{\alpha} - \underline{z}_g] \quad (\text{A.21})$$

where the scalars  $T_1$  and  $T_2$  are respectively

$$T_1 = \left[ \frac{\underline{z}_0^T \underline{z}_g}{\underline{z}_0^T \underline{z}_b} - \frac{(\underline{z}_0^T \underline{\alpha})(\underline{\alpha}^T \underline{z}_g)}{(\underline{z}_0^T \underline{z}_b)(\underline{\alpha}^T \underline{\alpha})} \right] \quad (\text{A.22})$$

$$T_2 = \left[ \frac{(\underline{\alpha}^T \underline{z}_g)}{(\underline{\alpha}^T \underline{\alpha})} \right] \quad (\text{A.23})$$

At the minimum of the function D, the gradient vanishes, that is  $\frac{\delta D}{\delta \underline{z}_1} = 0$ , and therefore

(A.21) becomes

$$\underline{z}_g = T_1 \underline{z}_b + T_2 \underline{\alpha} \quad (\text{A.24})$$

which implies that the vectors  $\underline{z}_g$ ,  $\underline{z}_b$  and  $\underline{\alpha}$  are linearly dependent.

Equation (A.21) is the gradient function corresponding to  $\lambda = \lambda_{\max}$ , the other candidate of  $\underline{\alpha}$  which must also be considered is the one corresponding to the minimum eigenvalue, that is  $\lambda = \lambda_{\min}$ , which has the form,

$$\underline{\alpha} = \underline{z}_1 - \lambda \underline{z}_0 \quad (\text{A.25})$$

Using a similar analysis, it can be shown that the gradient of the objective function under this condition has the form,

$$\frac{\delta D}{\delta \underline{z}_1} = \frac{1}{\|\underline{\alpha}\| \|\underline{z}_g\|} [\underline{z}_g - T_1 \underline{z}_b + T_2 \underline{\alpha}] \quad (\text{A.26})$$

where the scalars  $T_1$  and  $T_2$  are those defined in (A.22) and (A.23).

## Appendix B

**Table B-1:** Line data of 5-bus example #1

Line	From	To	Shunt Admittance	Series Impedance
1	1	4	$0.0 + j 0.0$	$0.05 + j 0.2$
2	1	5	$0.0 + j 0.0$	$0.05 + j 0.2$
3	2	4	$0.0 + j 0.0$	$0.05 + j 0.2$
4	2	3	$0.0 + j 0.0$	$0.1 + j 0.4$
5	2	5	$0.0 + j 0.0$	$0.1 + j 0.4$
6	3	5	$0.0 + j 0.0$	$0.15 + j 0.6$

**Table B-2:** Line data of 5-bus example #2

Line	From	To	Shunt Admittance	Series Impedance
1	1	2	$0.0 + j 0.025$	$0.08 + j 0.24$
2	1	5	$0.0 + j 0.015$	$0.04 + j 0.12$
3	2	3	$0.0 + j 0.010$	$0.01 + j 0.03$
4	2	5	$0.0 + j 0.020$	$0.06 + j 0.18$
5	3	5	$0.0 + j 0.020$	$0.06 + j 0.18$
6	3	4	$0.0 + j 0.025$	$0.08 + j 0.24$
7	4	5	$0.0 + j 0.030$	$0.02 + j 0.06$



**Table B-3: Line data of 14-bus example**

<b>Line</b>	<b>From</b>	<b>To</b>	<b>Shunt Admittance</b>	<b>Series Impedance</b>
1	1	2	0.0 + j 0.0	0.171 + j 0.348
2	1	6	0.0 + j 0.0	0.127 + j 0.270
3	2	3	0.0 + j 0.0	0.221 + j 0.200
4	2	9	0.0 + j 0.0	0.066 + j 0.130
5	3	9	0.0 + j 0.0	0.123 + j 0.256
6	4	5	0.0 + j 0.0	0.082 + j 0.192
7	4	9	0.0 + j 0.0	0.095 + j 0.199
8	5	6	0.0 + j 0.0	0.032 + j 0.085
9	6	8	0.0 + j 0.0	0.0 + j 0.110
10	6	11	0.0 + j 0.0	0.0 + j 0.556
11	7	8	0.0 + j 0.0	0.0 + j 0.176
12	8	11	0.0 + j 0.0	0.0 + j 0.209
13	9	10	0.0 + j 0.0	0.0 + j 0.252
14	10	11	0.0 + j 0.013	0.013 + j 0.042
15	10	13	0.0 + j 0.034	0.057 + j 0.174
16	10	14	0.0 + j 0.049	0.054 + j 0.223
17	11	12	0.0 + j 0.035	0.067 + j 0.171
18	11	13	0.0 + j 0.037	0.058 + j 0.176
19	12	13	0.0 + j 0.044	0.047 + j 0.198
20	13	14	0.0 + j 0.053	0.019 + j 0.059